The Influence of Bubbles on the Seasonal SAR Backscatter Response of Perennially Ice-Covered Lakes, Antarctica

Adam Gaudreau

Thesis submitted to the University of Ottawa
in partial Fulfillment of the requirements for the
Master of Science, Geography

Department of Geography, Environment and Geomatics
Faculty of Arts
University of Ottawa

Supervisor:

Dr. Denis Lacelle

Department of Geography, Environment and Geomatics, University of Ottawa

Thesis examiners:

Dr. Luke Copland

Department of Geography, Environment and Geomatics, University of Ottawa

Dr. Isaac Smith

Lassonde School of Engineering, York University

Abstract

Antarctica is home to numerous perennially ice-covered (PIC) lakes that host rich benthic microbial ecosystems. These lakes are covered by a thick floating ice cover year-round and often have water columns supersaturated in dissolved gases, resulting in heavily bubbled ice covers, altering the optical properties of the ice and the amount of light that penetrates into the water column. Thus, understanding the optical properties of perennial lake ice can have important scientific implications to the study of life on Earth and the search for extraterrestrial life. Synthetic aperture radar (SAR) remote sensing has been used rigorously for over 50 years to study and monitor the seasonal response and long-term trends of backscatter over seasonally ice-covered (SIC) Arctic lakes. Limited studies have assessed the impacts of dissolved gases and ice/water interface bubbles on SAR backscatter variability over SIC lakes. The seasonal backscatter response of Antarctic PIC lakes remains unexplored; their physical nature asserts that their backscatter response should largely be decoupled from seasonal factors according to SIC lake backscatter theory. Additionally, gas supersaturated PIC lakes are ideal candidates to better understand the role of gas buildup and bubble formation on the backscatter response from floating ice covers.

This thesis leverages a dense stack of Sentinel-1 C-band SAR imagery over Lake Untersee, a well-sealed PIC lake in East Antarctica, to explore the relationships between SAR backscatter and ice/water interface bubbles. This analysis integrates field measurements and temporal observations at the ice/water interface. Lastly, a brief comparative analysis extends to other ice covers, including moat-forming PIC lakes, as well as first-year and multi-year Arctic sea and lake ice. It is shown that Lake Untersee has a seasonal backscatter regime that is linked to air temperature. A strong correlation is found between the timing of backscatter intensity increase in winter and ice thickness. This relationship is attributed to variations in ice thickness which affect the length of the freezing period under the ice, the rate of dissolved gas accumulation, and ultimately, the nucleation and abundance of bubbles at the ice/water interface. These findings can be applied to other PIC lakes that have seasonal gas regimes. This research provides valuable insights into the complex interplay between ice cover characteristics, gas dynamics, interface bubbles, and SAR backscatter, enhancing our understanding of polar aquatic ecosystems and their broader implications for global environments.

Acknowledgements

First and foremost, I extend my heartfelt appreciation to Denis Lacelle, my thesis supervisor. His expertise, guidance, unwavering support, and incredible tolerance to my stubbornness have been instrumental in shaping the direction and quality of this research. His insightful feedback, dedication to my academic growth, and the countless hours spent discussing ideas have been invaluable. I am also thankful for his investments in my journey to Antarctica, which allowed me to participate in field research twice. Denis, your mentorship and the opportunities you provided me have been a driving force behind my academic achievements and personal growth.

In addition, I am immensely thankful to Dale Andersen, whose visions and generosity helped bring me to Antarctica. The two remarkable expeditions organized by Dale provided me with opportunities for exploration and learning. His passion for scientific history, discovery, and advancement, meticulous planning, and generosity have left a lasting mark on my personal and academic journey. Dale, your support and dedication have opened doors to experiences I will forever cherish.

I extend my sincere appreciation to the two esteemed examiners of my thesis proposal, Luke Copland and Claude Duguay. Their expertise in the subject matter led to specific and detailed lines of questioning and thoughtful feedback which helped guide the trajectory of my research and shape the final thesis. Thank you to Melanie Engram for sharing valuable insights and perspectives during a one-on-one discussion.

I would like to express my gratefulness for the financial support of the University of Ottawa (admissions scholarship), the TAWANI Foundation, the Trottier Family Foundation, and all other groups and individuals for their direct or indirect contributions that made my journeys to Antarctica and this research possible. I also extend great appreciation to Antarctic Logistics Centre International for their continued logistical support and accommodations that have made annual journeys to the Untersee Oasis possible for me and my colleagues.

Finally, I would like to thank my family and friends for their support throughout all my studies. Thank you to my mother and father, Clarice and Michel, for their support and encouragement to pursue higher education. Finally, a massive thank you to my partner, Sara-Emilie, for tolerating my work schedule and offering unconditional support and love during this process.

Table of Contents

List of Figures

List of Tables

Chapter 1: Introduction

1. General introduction

Polar lakes have global significance as they represent sentinels of climate change, are sources of greenhouse gases, and are refugia for diverse biological species and communities (Vincent & Laybourn-Parry, 2008). Lakes in Antarctica and their ecology are no exception, but unlike in the Arctic, most lakes in Antarctica develop a perennial ice cover. Perennially ice-covered (PIC) lakes are physically driven systems, and the presence of the ice cover affects their ecosystems. Ice cover thickness is typically in the 3-6 m range (Priscu et al., 1998) and reflects a balance between the conduction of energy out of the ice and the release of latent heat at the ice/water interface (McKay et al., 1985). Under steady state, the sublimation rate at the ice surface and freezing rate at the ice/water interface are in equilibrium, allowing for the ice cover to maintain a constant annual thickness (Faucher et al., 2019; McKay et al., 1985). In PIC lakes, the water column is often supersaturated in gases and bubble nucleation at the ice-water interface is the main process for removing gases in the presence of a well-sealed ice cover (Andersen et al., 1998; Craig et al., 1992). During freezing, bubble nucleation only occurs when the dissolved gas pressure exceeds the local hydrostatic pressure (c. 1.45 for a 5 m thick ice cover) and in this instance the freezing front can shift from a planar face to a dendritic growth pattern (Lipp et al., 1987). Analysis of the frequency distribution of occluded bubble content in an ice cover can preserve information about the freezing rate at the bottom of the ice cover (Faucher et al., 2019).

Perennial ice covers are also critical to the benthic phototrophic ecosystem (Andersen et al., 2011; McKay et al., 1994; Obryk et al., 2014; Parker et al., 1982; Priscu et al., 1998). In these lakes, the thickness of the ice cover and its optical properties controls the amount of light reaching the water column (scattering and absorption caused by liquid water, bubbles, and sediments) (McKay et al., 1994). Since the ice cover limits gaseous exchanges with the atmosphere, the freezing rates also affect the solute concentrations in the water column. Therefore, knowledge about the internal and seasonal properties of the perennial ice covers in Antarctica is important to assess the state of the aquatic ecosystems and global environments.

The phenology (onset and breakup) and thickness of the seasonal ice cover of Arctic lakes has attracted substantial monitoring because of their importance to local climate (Rouse et al., 2005) and economic activities (Mullan et al., 2017). However, the challenges of monitoring

lakes in polar regions have placed a greater importance on the remote collection of data. Radar techniques are commonly used because ice is highly transparent to radar energy. Currently, spaceborne active synthetic aperture radar (SAR) is widely used in studies on Arctic lake ice phenology (Murfitt & Duguay, 2021). By measuring the returned echo of emitted energy over large swaths and at regular repeat pass intervals, SARs produced dense temporal stacks of imagery that are used to track the evolution of the returned echo of lakes over time to infer lake ice phenology events. Many Arctic lakes show abrupt transitions in echo, or backscatter intensity, during the freezing season, marking the time when the lake ice cover freezes to the bottom. This phenomenon occurs as the ice cover couples with the lakebed, allowing a greater proportion of emitted energy to transmit into the lakebed sediment rather than returning to the sensor (Antonova et al., 2016; Duguay et al., 2002; Engram et al., 2013a; Jeffries et al., 1993). As such, long SAR backscatter records can help identify a long-term change in lake ice thickness and phenology characteristics (Engram et al., 2018; Morris et al., 1995).

Most SAR studies have focused on shallow Arctic lakes with seasonal and relatively shallow ice covers that ground, leaving the backscatter response of deeper ice-covered lakes relatively unexplored (Morris et al., 1995; Murfitt & Duguay, 2021). In addition, none have explored the seasonal SAR backscatter regimes of Antarctic PIC lakes. The later may be under the assumption that there are limitations in describing the backscatter mechanisms of PIC lakes on the basis that: (1) most perennial ice covers do not ground to the lakebed, and (2) perennial ice covers are often stratified with several horizons of heavily bubbled ice. Based on these physical attributes, any abrupt transitions in SAR backscatter intensity observed over PIC lakes necessitates a different backscatter hypothesis to the one used for lakes with a seasonal and grounding ice cover. Given dissolved gas supersaturation can lead to the spontaneous nucleation of bubbles in PIC lakes (Andersen et al., 1998; Craig et al., 1992), the mechanism for backscatter evolution might relate to the development of roughness at the ice/water interface from bubbles (Gunn et al., 2018). Many environmental factors that create noise when deriving lake ice phenology through SAR backscatter in Arctic lakes are negligeable or completely absent in many Antarctic PIC lake environments, including open water, snow cover, slush, and ice break-up, among others (Murfitt & Duguay, 2021). Therefore, the large and deep PIC lakes in Antarctica represent ideal subjects to improve our knowledge of lake ice backscatter sources and mechanisms.

The aim of this thesis is to provide a first look into previously undocumented SAR backscatter regimes over PIC lakes in Antarctica. Because this remains virtually undocumented over PIC lakes, the observed phenomenon is discussed in the context of seasonally ice-covered (SIC) Arctic lakes where similar phenomena have been widely documented and discussed in the literature. This thesis focuses on a PIC lake, called Lake Untersee, located in the Untersee Oasis, East Antarctica which is unique from other PIC lakes on the continent in that it maintains a well-sealed ice cover which does not develop a moat in the summer season (Faucher et al., 2019, 2021). A dense stack of Sentinel-1 C-band SAR imagery is used to describe the backscatter time series and spatio-temporal phenomena over the lake. The backscatter discussions are supported by observations made below the ice cover as well as by physical ice cover measurements. This thesis also aims to give a brief comparative analysis of backscatter over other Antarctic PIC lakes and Arctic ice covers.

For the remainder of Chapter 1, a brief introduction to radar and SAR for geotechnical purposes is given, followed by the application of SAR for the purpose of studying lake ice. The primary findings of this thesis are presented in Chapter 2 in the form of a journal manuscript formatted for publication in Communications Earth & Environment. Chapter 3 elaborates on the findings of the journal manuscript by incorporating the backscatter over other ice covers in a brief comparative analysis, and additionally includes special backscatter observations made over Lake Untersee and Lake Obersee, the neighbouring PIC lake in the Untersee Oasis. Concluding remarks to this thesis are given in Chapter 4.

2. A brief on synthetic aperture radar

Radar (**ra**dio **d**etection **a**nd **r**anging) operates in the radio wave, or radio frequency, and microwave frequency domains (3 kHz to 300 GHz) of the electromagnetic (EM) spectrum. At their most basic, active geotechnical radars aim to measure the partial return (backscatter) between the emitted and received EM radiation power at their antenna. Because radio waves have long wavelengths (inversely proportional to their frequency), the EM radiation can penetrate materials to different depths depending on the wavelength and the electrical resistivity and permittivity of the material. Thus, depending on these characteristics, radar energy may backscatter from both the surface and the sub-surface.

Like optical sensors, imaging radars can form images of their target, but at radar frequencies. Earth-observing active imaging radars build up backscatter images of the earth by emitting EM pulses in the antenna slant range direction (**Fig.1**), also know as the cross-track direction, and recording the backscatter as the radar platform moves in the azimuth direction, also know as track direction. The spatial resolution of the formed image varies in these two directions: the cross-track resolution is determined by the pulse bandwidth, and the along-track resolution is determined by the length of the antenna in the track direction. In the case of the synthetic aperture radar (SAR), the motion of the platform in the along-track direction is utilized to synthetically increase the size of the antenna, thus providing improved along-track resolution over a stationary antenna of the same size. SARs also make use of pulse frequency modulation (chirp) to improve their cross-track resolution over radars without pulse frequency modulation.

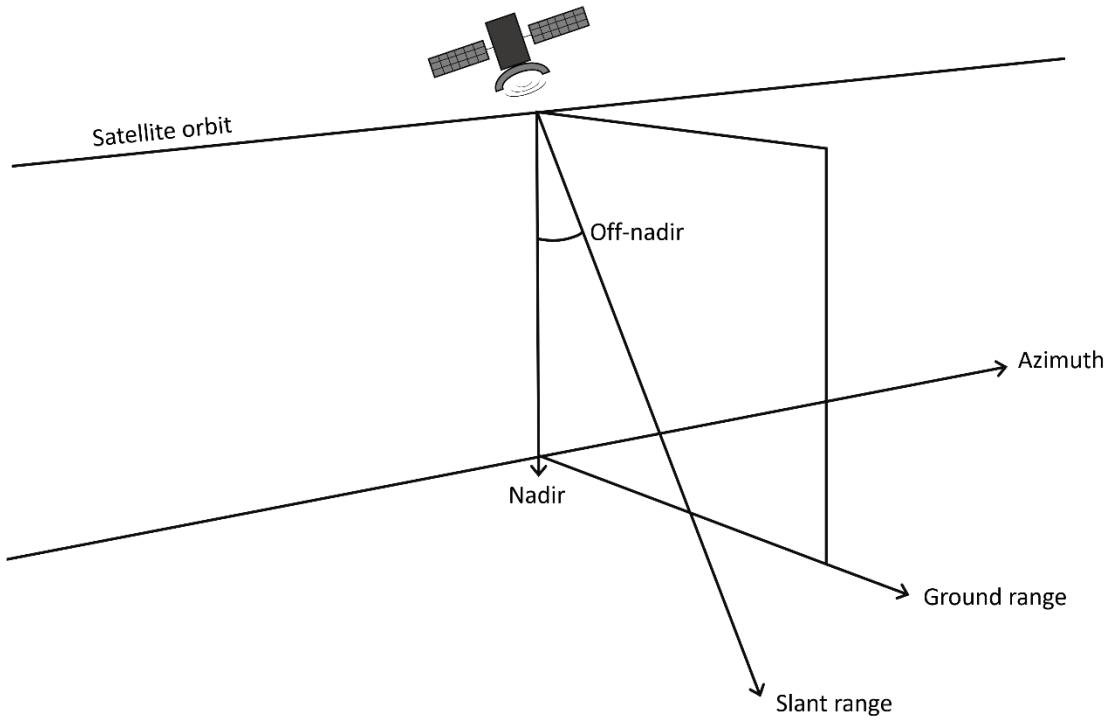

Fig. 1 Common SAR satellite viewing terminology. The azimuth direction, or along-track direction, is the same as the satellite orbit velocity vector. The cross-track direction, or ground range direction, is perpendicular to the azimuth. The direction along the line-of-site (LOS) is the viewing angle of the antenna off the nadir position, also called the slant-range direction.

SARs can be characterized by the polarization of the transmitted and received EM wave. Polarization refers to the vector of the electric field (EF) relative to the plane of incidence; a horizontal polarization EM wave has EF normal (perpendicular) to the plane, while vertical

polarization has EF within (parallel) the plane. SARs have two primary polarization regimes: co-polarization refers to signal transmission and reception with EF in the same orientation (horizontal-horizontal: HH, and vertical-vertical: VV), and cross-polarization refers to signal reception with opposite EF orientation compared to the transmitted signal (horizontal-vertical: HV, and vertical-horizontal: VH). A SAR platform can be configured to acquire imagery in numerous polarization regimes, including single (HH or VV), dual (HH and HV or VH and VV), or quadrature/fully-polarimetric (HH, VV, HV, and VH). By controlling the polarization of the emitted energy and subsequently measuring the power of the returned reflection in different polarizations, additional information about the surficial and internal properties of the scattering body can be extracted, including their dominant scattering mechanism and structural orientation.

The EM wave interaction is directly proportional to the scatterer properties, notably the relative permittivity and surface roughness. Here, because the loss component of the relative permittivity is low for ice, it is not considered. The relatively permittivity of a material ε' is the measure of its polarizability given an applied electric field, whereby a material with high ε' will polarize more than a material with low ε'. The relative permittivity of a material can be highly temperature and frequency dependent. For common SAR frequencies used in the study of lake ice, the relative permittivity of ice typically takes a value of $\varepsilon' = 3.17$ (Matzler & Wegmuller, 1987). Water, on the other hand, shows a greater frequency dependence, whereby at 0 °C, ε' = c. 90, 40, and 20 for C- (4.0–8.0 GHz), X- (8.0–12.0 GHz), and Ku- (12.0–18.0 GHz) band (Meissner & Wentz, 2004). The relative permittivity of air takes a value of $\varepsilon' = 1.0006$. A relative permittivity mixture formula (weighted averaging) can be used as a first-order approximation of the effective (bulk) dielectric permittivity ε'_e of mixed materials:

$$\varepsilon'_e = \sum_i \varepsilon'_i \varphi_i \tag{1}$$

where ε'_i and φ_i are the respective dielectric permittivity and volumetric fraction of the pure unmixed materials.

The overall proportions of the reflected and transmitted components of the emitted EM wave after an interaction with incident materials can be solved with the Fresnel equations. In the

presence of non-conductive materials, both components can be solved by considering only the refractive index n of a material:

$$n = \sqrt{\varepsilon'} \tag{2}$$

Backscatter intensity increases when the refractive index of incident materials above and below an interface, for example n_1 and n_2, are increasingly dissimilar. The coefficients of reflection for s polarization (horizontal polarization) R_s and p polarization (vertical polarization) R_p EM waves are given with:

$$R_s = \left| \frac{n_1 \cos\theta_i - n_2 \cos\theta_t}{n_1 \cos\theta_i + n_2 \cos\theta_t} \right|^2 \tag{3}$$

$$R_p = \left| \frac{n_1 \cos\theta_t - n_2 \cos\theta_i}{n_1 \cos\theta_t + n_2 \cos\theta_i} \right|^2 \tag{4}$$

where θ_i is the EM wave angle of incidence upon an interface and θ_t is the EM wave angle of transmission after passing through the interface, given with Snell's law:

$$n_1 \sin\theta_i = n_2 \sin\theta_t \tag{5}$$

The coefficients of transmission for s polarization T_s and p polarization T_p are then given with:

$$T_s = 1 - R_s \tag{6}$$

$$T_p = 1 - R_p \tag{7}$$

When the EM wave impinges perpendicular to an interface such that θ_i = 0 °, no distinction is made between s and p wave polarization and the coefficients of reflection R and transmission T are simplified:

$$R = \left|\frac{n_1 - n_2}{n_1 + n_2}\right|^2 \quad (8)$$

$$T = 1 - R \quad (9)$$

Equations (8) and (9) are generally true for down-firing radars, such as GPRs, while equations (3) to (7) are true for side looking radar, such as SARs, where the angle of incidence is commonly between c. 15 and 45 ° off the nadir orientation. For SARs, the change in EM radiation intensity between emission P and reception P_0 is commonly expressed in decibels (dB):

$$dB = 10 \log_{10}\left(\frac{P}{P_0}\right) \quad (10)$$

3. SAR over lake ice

Active SARs, typically spaceborne, operate by measuring the instantaneous phase and amplitude of the returned signal from individual ground resolution cells over large swaths. Common SAR wavelengths have non-negligeable penetration in ice which introduces significant bias to the retrieval of topographic and deformational interferometric height (Groh et al., 2014; Rignot et al., 2001; Weber Hoen & Zebker, 2000). Conversely, this penetration has enabled the monitoring of lake ice properties and has given rise to a long history in the detection and monitoring of lake ice phenology and grounding regimes (Elachi et al., 1976; Jeffries et al., 1993; Sellmann et al., 1975). The ability to acquire data in poor lighting and weather conditions have made spaceborne SAR platforms the most widely used in studies of lake ice compared to optical platforms (Murfitt & Duguay, 2021).

Pioneers studying lake ice with radar backscatter attributed differences in backscatter intensity over lake ice to whether an ice cover was floating or frozen to lakebed sediment. Lakes with low backscatter intensity were known to freeze completely to the lakebed, whereas lakes with high backscatter intensity were deeper lakes used as winter water supplies by nearby communities (Sellmann et al., 1975). These observations were further validated with ice cores to determine whether the lake ice was floating (Weeks et al., 1978). The theoretical basis for this association was rooted in the electrical properties (i.e., dielectric permittivity) of the materials the EM wave interacts with as it was previously theorized that the internal and basal properties of ice

could be inferred (Bryan & Larson, 1973, 1975). The larger dielectric contrast between ice and water gives a high reflection coefficient, while the smaller dielectric contrast between ice and frozen lakebed sediment gives a low reflection coefficient. However, it was also postulated that the smooth surface of an ice/water interface would create specular reflections, meaning EM wave must impinge on radiometrically rough surfaces to produce the observed backscatter. Thus, it was suggested that vertically oriented bubbles within the lake ice reflects the incident waves towards the ice/water interface where the high dielectric contrast at the ice/water interface reflects part of the waves towards the antenna (Weeks et al., 1978). This mechanism, commonly referred to as the double bounce hypothesis in the literature, became the widely accepted hypothesis to explain high backscatter over lake ice (Duguay et al., 2002; Jeffries et al., 1993, 1994; Morris et al., 1995) and river ice (Gherboudj et al., 2010; Leconte & Klassen, 1991).

SAR backscatter is widely used to study Arctic lake ice because key lake ice phenology events are associated with characteristic backscatter intensity signals. Notably, backscatter time series of Arctic lakes have shown significant drop-offs in backscatter intensity during the winter season, and the mechanism responsible has been linked to the coupling of the lake ice cover with the lakebed sediment. The theoretical basis for the backscatter drop-off phenomenon is elaborated below in conjunction with the schematic in **Fig. 1** and the effects on a time series of backscatter in **Fig. 2**.

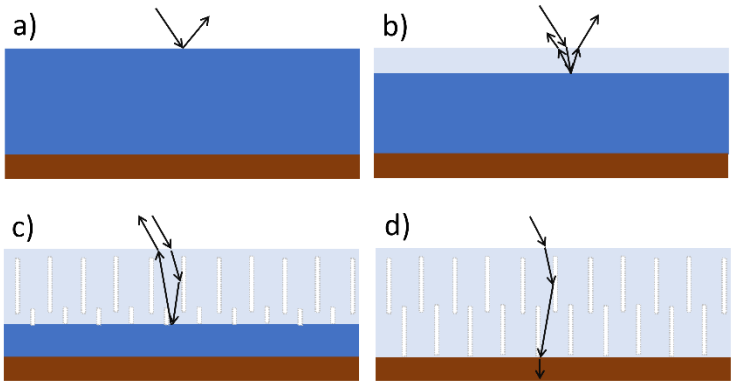

Fig. 2 Schematic of backscatter from lake ice. Commonly accepted SAR backscatter regime of Arctic lake ice: **a)** specular reflection off open water, **b)** surface bounce at air/ice and ice/water interface, **c)** double bounce off columnar bubbles and ice/water interface, and **d)** reflection off columnar bubbles and transmission into underlying frozen sediment.

Backscatter intensity is initially low on (calm) open water due to the specular reflection of the incident EM wave away from the antenna (**Fig. 2a** and **Fig. 3a**). As ice begins to form,

increased intensity is attributed to the increased dielectric contrast between the atmosphere (ε' of air = 1) and the ice surface (ε' of ice = 3.17) (**Fig. 2b** and **Fig. 3b**) but remains relatively low because undeveloped ice is relatively smooth and specular. This stage is typically described with intensities ranging anywhere between –4.8 dB (Surdu et al., 2015) and –22 dB (Jeffries et al., 1993) at C-band. As freezing continues and the ice cover develops further, gases incorporate into the ice volume as columnar bubbles, providing an array of dielectrically contrasted interfaces for double-bounce reflections between the bubble and the high dielectric permittivity of water (ε' of water ≈ 90 at C-band) (**Fig. 2c** and **Fig. 3c**), resulting in characteristically high backscatter intensities for floating ice. This period can have intensities that are temporally much more stable (Antonova et al., 2016), generally between –9 dB and 2 dB (Duguay et al., 2002). Then, for shallower lakes that experience ice cover grounding, a sudden drop-off in backscatter intensity is commonly observed and attributed to the coupling of the ice cover with the underlying sediments (**Fig. 2d** and **Fig. 3d**). Because frozen or thawed lakebed sediment has a relatively low dielectric permittivity compared to water (c. 7 compared to 90 at C-band), the double-bounce component is largely eliminated because a greater proportion of energy can transmit and dissipate into the lakebed sediment. This period shows mid- to low-range backscatter intensities with drop-offs of 11.8 dB (Morris et al., 1995) or more. This general backscatter regime has been recorded in numerous studies (e.g., **Fig. 3**).

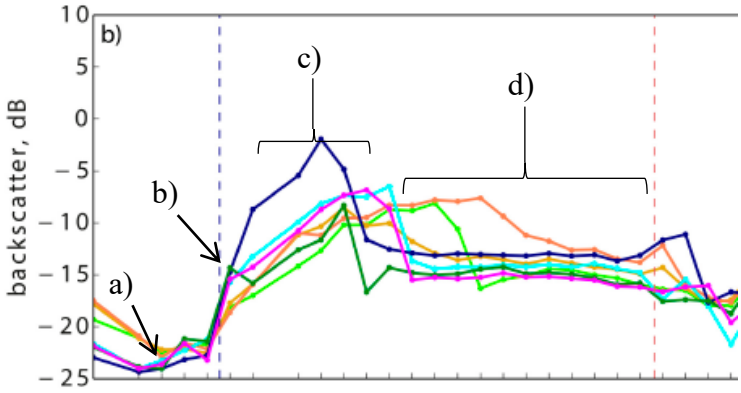

Fig. 3 Backscatter time series over lake ice. a) specular reflection off open water, **b)** surface bounce at air/ice and ice/water interface, **c)** double bounce between columnar bubbles and ice/water interface, and **d)** reflection off columnar bubbles and transmission into underlying sediment. Blue line is first negative temperature in fall and red lines is first positive temperature in spring. See Antonova et al. (2016) for complete figure.

The dominant backscatter sources in lake ice can also be derived in a simplified manner by substituting the above-mentioned relative permittivity for air, ice, water, bubbled ice

dielectric mixtures, and sediment into equation (7) and (8). The interaction of an EM wave transiting from air into a body of ice with possible internal bubble horizons and underlying water is such that the coefficient of reflection is greatest for internal horizons or the ice/water interface. If a grounding component is included, the relative permittivity of thawed or frozen lakebed sediment acts to decrease the coefficient of reflection, thus increasing the coefficient of transmission. Note that deriving the SAR scattering source in this way is simplified by using Fresnel equations for nadir-firing radars. In reality, looking geometry and polarization must be considered with equations (2) and (3), although similar results are obtained.

Most studies have described lake ice backscatter from single co-polarization SAR imagery, leaving the fully-polarimetric responses of lake ice relatively undescribed. Analyzing EM polarization between emission and reception is important when accurately interpreting scattering mechanisms, be it surface, double bounce, or volumetric. Freeman & Durden (1998) make several conclusions regarding the fully-polarimetric response of a surface: only volume scattering can depolarize a signal, meaning analyses of single co-polarization responses only provides little insight on volumetric scattering. To interpret volumetric scattering, cross-polarization responses (HV or VH) are needed. Additionally, the co-polarization relationship can be used to determine whether surface bounce (large HH+VV) or double-bounce (large HH-VV) dominates the response, and the dual co-polarization ratio (HH/VV) should be near unity if surface bounce is the dominant mechanism. Therefore, determination of the relative contributions of lake ice scatterers requires comprehensive fully-polarimetric analyses such as the Yamaguchi three-component decomposition (Yamaguchi et al., 2005).

Recently, the availability of fully-polarimetric SAR imagery has challenged the commonly accepted mechanism of lake ice backscatter. Despite the presence of columnar bubbles in the ice cover, Atwood et al. (2015) showed that the largest contribution to backscatter intensity in floating lake ice is a surface bounce derived from the ice/water interface. These findings were supported with several fully-polarimetric analyses of SAR imagery over lake ice: Yamaguchi three-component decomposition showed surface bounce as the dominant mechanism, the co-polarization ratios were near unity, and the co-polarization phase difference was 0 °. Additionally, the authors used a ground-based fully-polarimetric X- and Ku-band scatterometer to measure in situ backscatter intensity as a function of angle of incidence. Their results show distinct intensity peaks at range distances associated with the lake ice surface and bottom, but not

for the ice volume, suggesting top surface or bottom surface scattering were the dominant mechanisms. Atwood et al. (2015) also modeled microwave interactions with a simulated floating ice cover, showing that backscatter intensities would only increase when the ice/water interface was rough. Without surface roughness, the double bounce signal remained below the theoretical noise threshold (Atwood et al., 2015).

These findings were reiterated by Gunn et al. (2018) when additional scatterometer and SAR analysis lead to similar conclusions. Gas bubbles extending from the termini of columnar bubble inclusion at the ice/water interface were also observed by Gunn et al. (2018), which they suggest provided sufficient roughness, faceting, and height deviation to satisfy the Fraunhofer roughness criterion to eclipse microwave wavelengths (Ulaby & Long, 2014). These findings are consistent with those of Engram et al. (2012) for the L-band interactions over lake ice which showed that the single bounce component of a Pauli decomposition supports surface scatter from large methane ebullition bubbles at the ice/water interface as the dominant scattering mechanism. The findings presented by Engram et al. (2012), Atwood et al. (2015), and Gunn et al. (2018) provide alternative idea to the long-standing double-bounce hypothesis of Arctic lake ice backscatter.

4. Study location

4.1. Antarctic setting

East Antarctica, specifically the Queen Maud Land (Dronnin Maud Land) region, is home to the Untersee Oasis, an intriguing geological enclave situated within the Gruber Mountains of the Princess Astrid Coast. Glacial retreat in the Untersee Oasis began c. 12 to 10 kyr ago, coming to current configuration c. 6 kyr ago (Schwab, 1998). During the period of glacial retreat, two PIC lakes, called Lake Untersee and Lake Obersee, developed in the glacial scour depressions (**Fig. 4**). The Gruber Mountains surround Lake Untersee to the west, south, and east, towering between 600 and 2790 m over the lake.

Lake Untersee (13.47 °E, 71.34 °S) and Lake Obersee (13.66 °E, 71.28 °S) are found at c. 612 and c. 756 m, respectively, above sea level (Schwab, 1998), and located c. 7 km distance from each other in the Untersee Oasis. Meteorological measurements (2008 to 2017) along the

shoreline of Lake Untersee yielded a mean annual air temperature of –9.5 °C ± 0.7 °C, with average summer month (December, January, and February) temperatures of c. –2.65 °C and thaw degree-days ranging from 7 to 51 (Andersen et al., 2015; Faucher et al., 2019). Despite having a relatively warm mean annual air temperature for Antarctica, the climate in the oasis is dominated by intense sublimation that limits surface melting due to cooling associated with the latent heat of sublimation (Hoffman et al., 2008).

4.2. Lake Untersee

Lake Untersee has a surface area of c. 11.4 km^2 (c. 6.5 km by c. 2.5 km) and a volume of 5.21 × 10^8 m^3 (Faucher et al., 2021), making it one of the largest freshwater lakes in central Dronning Maud Land (Hermichen et al., 1985). The closed-basin lake is dammed by the Anuchin Glacier to the north where a pressure ridge forms at contact points between lake and glacier ice. The lake has a perennial ice cover that does not develop a moat during the summer, and as such the water column remains well-sealed from the atmosphere (Faucher et al., 2019, 2021). The ice surface is highly pitted with deep scallops from ablation and wind erosion. With the exception several large boulders scattered across the lake and a boulder field at the southern end of the lake, the surface is free of fine sediments. The ice cover thickness varies between 1.96 and 3.96 m (Faucher et al., 2019). The ice cover contains bubbles of various morphologies (spherical, oval, dendritic, and tubular), at times occupying as much as 50 % by volume (between 2 and 50 %), and modeled ice density over the entire ice cover is 891 ± 5 kg m^{-3} (Faucher et al., 2019). Measurements of ice cover thickness at the same location has remained constant ± 0.07 m over a 6-year period, suggesting the ice cover is in equilibrium steady-state, where ablation and freezing rates are similar (Faucher et al., 2019). In fact, measured ablation in the central and southern regions of the lake yielded values of c. 40 and c. 75 cm yr^{-1}, respectively, while ice accretion rates derived from frequency distribution of bubble content and $\delta^{18}O$ values for the same regions yield 49 and 91 cm yr^{-1}, respectively (Faucher et al., 2019).

The lake has two sub-basins separated by a sill: 1) a large basin occupies the northern and central sectors to a maximum depth of 169 m, and 2) a shallower basin occupies the southern sector to a maximum depth of 100 m (Wand et al., 1996). The water in the larger and deeper basin and above the southern basin is well mixed and has a temperature of c. 0.5 °C, pH of c. 10.6, dissolved oxygen (DO) of c. 150 %, and electrical conductivity of c. 503 µS cm^{-1}

(Andersen et al., 2011; Marsh et al., 2020; Wand et al., 1997, 2006). In the southern sector between c. 80 and 100 m depth, the water is physically and chemically stratified, with temperatures between c. 3.6 and 4.5 °C, pH between c. 6.1 and 7.5, DO near 0 %, and electrical conductivity between c. 524 and 1500 µS cm^{-1} (Wand et al., 1997, 2006). Lake Untersee is recharged by subaqueous meltwater and subglacial meltwater of the Anuchin Glacier (Faucher et al., 2019). Sporadic glacial lake outburst floods originating from Lake Obersee also recharge Lake Untersee with water and nutrients (Faucher et al., 2021).

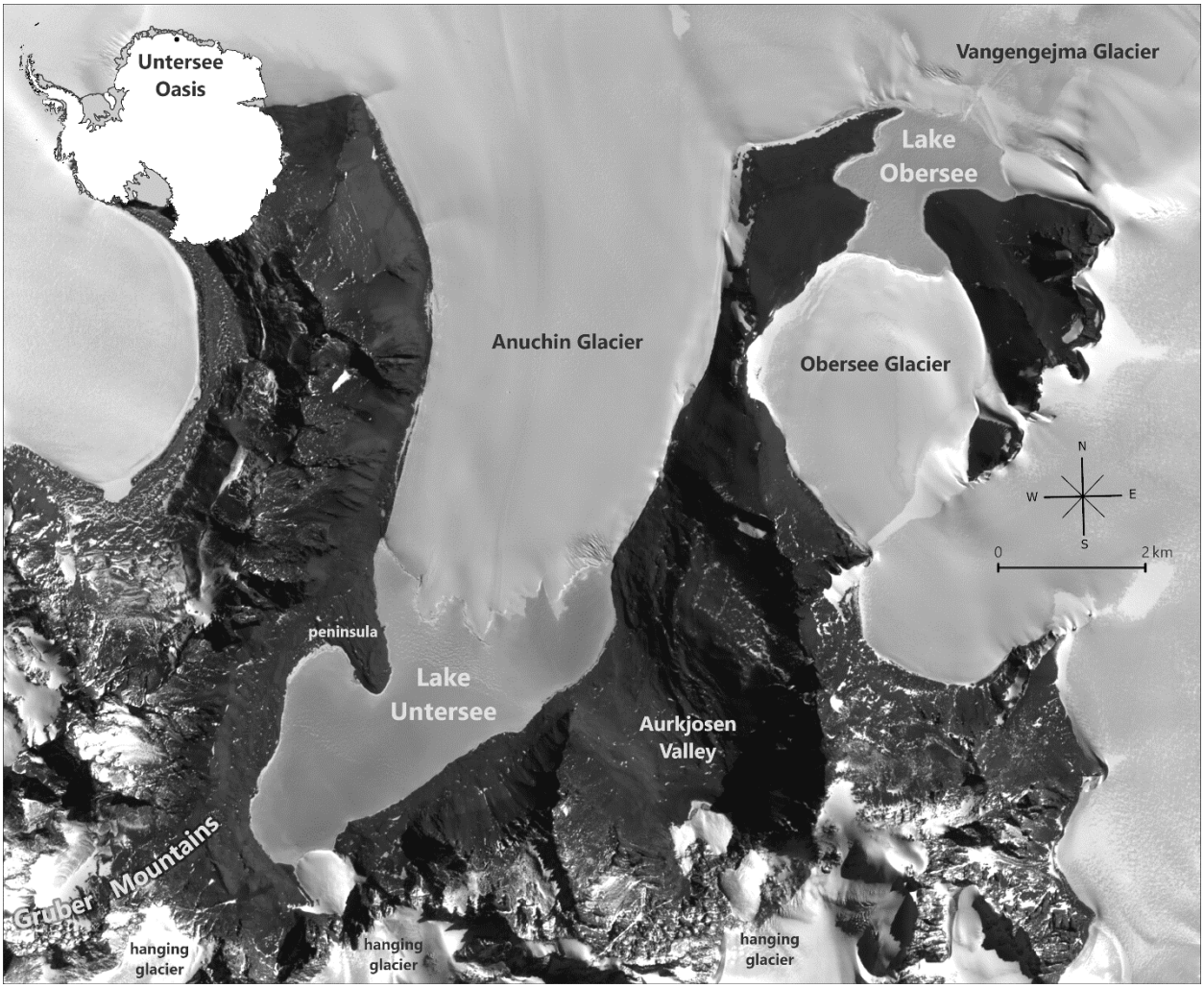

Fig. 4 Lake Untersee and Lake Obersee in the Untersee Oasis. Glacially dammed Lake Untersee and Lake Obersee in the Untersee Oasis, Gruber Mountains of East Antarctica. Greyscale background is band 4 of Sentinel-2 MSI acquired on 12 January 2018, courtesy of ESA. Map generated using ArcGIS Pro.

Chapter 2: Bubbles at the Ice/Water Interface of an Antarctic Perennially Ice-Covered Lake Cause Abrupt Seasonal SAR Backscatter

Adam Gaudreau[1,*], Denis Lacelle[1,*], Dale Andersen[2]

*Corresponding author

Communications Earth & Environment

Abstract. This study examines synthetic aperture radar (SAR) backscatter characteristics over Lake Untersee, a deep lake in Antarctica with a perennial and floating ice cover. Sentinel-1 C-band SAR imagery was used for visual observations and time series analysis of backscatter over the lake, while video footage beneath the ice aided in characterizing roughness at the ice/water interface. Lake Untersee exhibits regular, seasonally-driven patterns of backscatter intensities. The video footage reveals bubbles under the ice that can produce backscatter. A strong correlation is found between the timing of backscatter intensity increase in winter and ice thickness. This relationship is attributed to variations in ice thickness which affect the length of freezing period under the ice, the rate of dissolved gas accumulation, and ultimately, the abundance of bubbles. This research provides valuable insights into the relationship between subaqueous process below lake ice and SAR backscatter, contributing to a better understanding of polar lakes.

Key words: Synthetic aperture radar (SAR), Antarctica, perennially ice-cover lake, bubbles, dissolved gas

1. Introduction.

The perennial ice-covers of Antarctic lakes is an important feature that influences the biogeochemistry of the water column and the benthic microbial ecosystem (Vincent & Laybourn-Parry, 2008). The thickness of perennial ice covers, typically in the 3-6 m range (Priscu et al., 1998), is maintained by the equilibrium between water freezing onto the bottom of the ice cover and its ablation at the surface (McKay et al., 1985). The water column of perennially ice-covered (PIC) lakes is often supersaturated in gases, with the saturation level mainly determined by the thickness of the ice cover and its effect on hydrostatic pressure. As water freezes to the bottom of the ice cover, the gases are exsolved, and the gas supersaturation level increases in the boundary layer (Andersen et al., 1998; Craig et al., 1992; Lipp et al., 1987). Once a critical gas saturation threshold is reached, bubble nucleation can take place at the ice/water interface. The gas bubbles then become included in the accreting ice and are eventually released to the atmosphere from the ablation of the ice cover (Andersen et al., 1998; Craig et al., 1992). The thickness and bubble content of the ice covers are thus critical to the benthic phototrophic ecosystem as they affect the optical properties (scattering and absorption caused by bubbles and sediments) of the ice cover and, by consequence, the amount of light reaching the water column (McKay et al., 1994). Therefore, knowledge about the spatial and temporal changes in internal optical properties of the perennial ice covers, including bubbles, in Antarctica is important to assess the state of the aquatic ecosystems and global environments.

Synthetic aperture radar (SAR) imagery has been used to infer the conditions at the ice/water interface as well as to determine the phenology and grounding regimes of ice covers of Arctic lakes. Early studies attributed high backscatter over Arctic lake ice to a double bounce interaction between inclusions of vertically oriented tubular bubbles within the ice and the high dielectric contrast at the ice/water interface (Weeks et al., 1978). Subsequent studies have used this interaction to infer lake ice phenology (freeze-up and break-up) from temporal changes in the backscatter intensity signal in dense stacks of SAR imagery (Antonova et al., 2016; Duguay et al., 2002; Morris et al., 1995; Murfitt & Duguay, 2020; Surdu et al., 2015). The grounding regimes of lake ice were similarly inferred from abrupt drop-offs in SAR backscatter time series because the lower dielectric contrast at an ice/sediment interface allows more energy to be transmitted into the lacustrine sediments rather than returning to the sensor (Antonova et al., 2016; Engram et al., 2018; Jeffries et al., 1993). However, Gunn et al. (2018) recently found that

bubbles at the ice/water interface of floating lake ice cover are also able to produce the necessary roughness for high backscatter at C-band wavelengths. This discovery suggest that high backscatter can occur independently of the inclusion of vertical bubbles within ice covers. However, studies have yet to evaluate the effect of bubbles at the ice/water interface on the spatial and temporal variability of SAR backscatter despite early works that suggested that variations in dissolved gas content in the water column affects the formation of ice/water interface bubbles and the backscatter intensities (Jeffries et al., 1994; Mellor, 1982).

Perennially ice-covered lakes in Antarctica are ideal candidates to assess the role of gas buildup and the development of bubbles at the ice/water interface on a time series of SAR backscatter intensities. These lakes have water columns that are supersaturated in gases and a floating ice cover that contain a range of bubble morphologies (Adams et al., 1998; Faucher et al., 2019; McKay et al., 1994). As such, their SAR backscatter time series should be unaffected by phenology and grounding regimes. Here, we examine the spatio-temporal evolution of SAR backscatter over Lake Untersee, a large PIC lake in central Queen Maud Land, East Antarctica (Hermichen et al., 1985). From a dense stack of Sentinel-1 C-band SAR imagery acquired between 2019 and 2023 combined with field measurements and temporal observations at the ice/water interface, we examine the potential relations between C-band SAR backscatter and ice/water interface bubbles. Lastly, backscatter intensities over Lake Untersee are compared with other ice covers, including moat-forming PIC lakes and the first-year (FY) and multi-year (MY) ice of sea ice and an Arctic lake with a seasonal ice-cover (SIC). Our results show that Lake Untersee displays regular seasonal oscillations of backscatter intensity linked to seasonal differences in the abundance of bubbles below the ice cover, a process dependant on the period of ice freeze-on at the ice/water interface.

2. Methods and Materials.

Study site. Lake Untersee (71.34 ° S, 13.47 ° E) is located c. 612 m above sea level in the Gruber Mountains of East Antarctica (**Fig. 5**). Between 2008 and 2019, a meteorological station located on the shoreline of Lake Untersee reported a mean annual air temperature of –9.5 °C ± 0.7 °C and a mean relative humidity of 42 ± 5 % (Andersen et al., 2015; Faucher et al., 2019). Despite having a relatively warm mean annual air temperature for Antarctica, the climate is dominated by intense sublimation that limits surface melting due to cooling associated with the

latent heat of sublimation (Hoffman et al., 2008). The average wind speed is 5.4 m s^{-1} and are dominated by persistent southerlies that descend from the overhead glaciers in the south and sweep across the lake (Andersen et al., 2015).

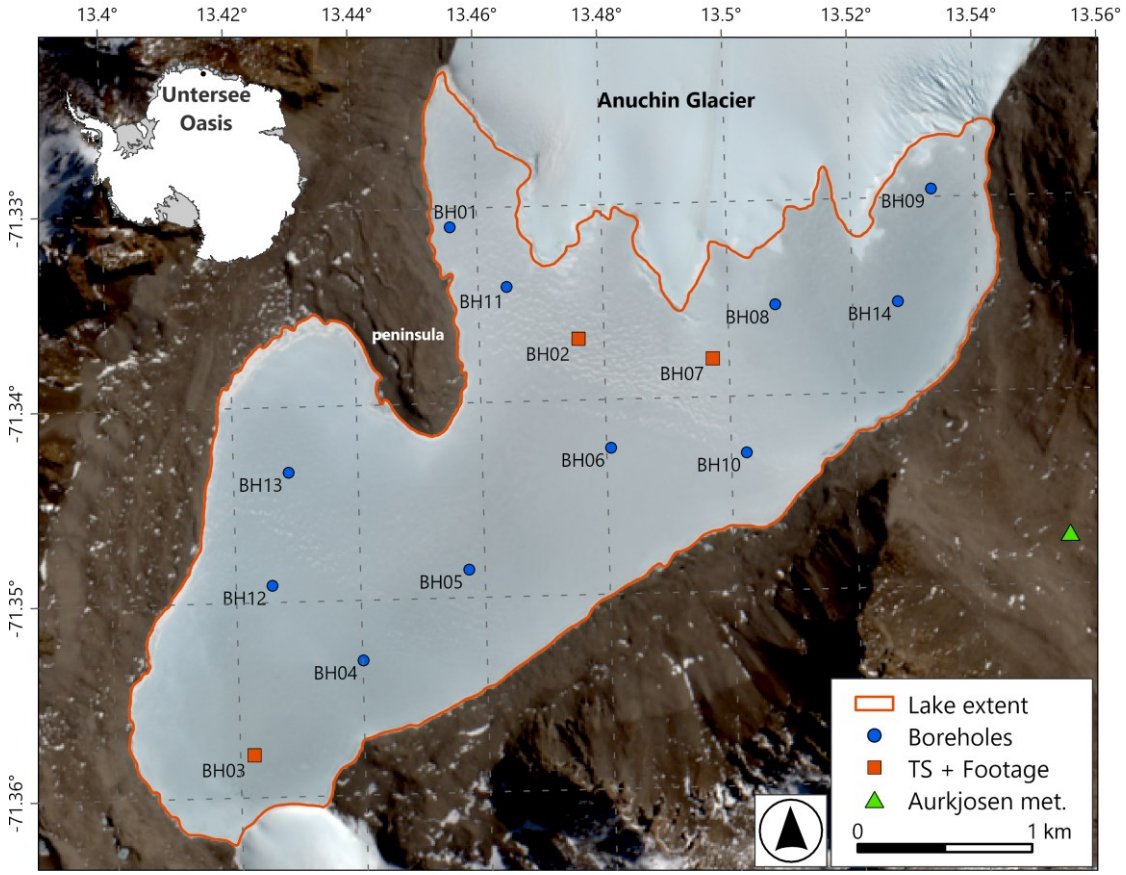

Fig. 5 Lake Untersee, Dronning Maud Land, East Antarctica. Location map showing the ice cover outline (orange line), the location of boreholes (BH) where water depth, ice thickness, and freeboard were measured (blue circle), "TS + Footage" are the BH locations used for backscatter time series analysis and where ice/water interface footage was captured (orange square), and the meteorological station in the Aurkjosen Valley just east of the lake (green triangle). Inset is the location of the Untersee Oasis relative to continent of Antarctica. Background is Sentinel-2 MSI acquired on 12 January 2018, courtesy of ESA. Map generated using ArcGIS Pro.

Lake Untersee has a surface area of approximately 11.4 km^2 and a volume of c. 5.21 × 10^8 m^3 (Faucher et al., 2021). The ice cover has an average thickness of c. 2.77 m (ranges between 1.96 and 3.96 m), and the thinnest ice cover are found in areas exposed to persistent winds that enhance sublimation (Andersen et al., 2015; Faucher et al., 2019). The ice cover of Lake Untersee is in steady state because ice thickness measurements from the same location showed little variation over a 6-year period (± 0.07 m). This indicates that the freezing and

ablation rates of the ice cover must be near equal (i.e., McKay et al., 1985). Measurements from ablation ropes provided ablation rates of c. 40 ± 1.2 cm yr^{-1} and c. 75 ± 4.2 cm yr^{-1} in the northern and southern sectors, respectively, which are comparable to freezing rates estimated from δ18O profiles in the ice cover (Faucher et al., 2019) . The entire surface of the ice cover remains rough year-round with sun cups c. 5 cm in depth and 10 cm wide present at the surface, formed through a combination of melting, sublimation, and wind erosion. The ice cover contains bubbles of various morphologies (spherical, oval, dendritic, and tubular), at times occupying as much as 50 %vol (Faucher et al., 2019). The bubbles span a range of lengths and diameters, commonly exceeding 1 m in length and 1 cm in diameter. Summer heating of the ice promotes the formation of Tyndall figures near the surface (McKay et al., 1994) resulting in whiter ice with increased optical scattering.

The lake is glacially dammed at its northern sector by the Anuchin Glacier and is recharged by sub-aqueous melting of the glacier and a subglacial meltwater source (Faucher et al., 2019). The sub-aqueous meltwater from the glacier directly introduces ice-entrapped air into the water column. The lake has two sub-basins: a large northern oxic basin reaching a maximum depth of 169 m and a smaller southern basin with a maximum depth of 100 m in which the water becomes anoxic below the depth of a dividing sill around 60 m. The oxic water is well mixed on a monthly timescale (Steel et al., 2015) and is supersaturated in gases with dissolved oxygen (DO) reaching 150 %, a value consistent with the hydrostatic pressure caused by the ice cover (Andersen et al., 2011; Marsh et al., 2020; Wand et al., 1997, 2006). Gas bubbles are commonly observed at the ice/water interface, ranging from a few millimeters to meters in diameters. On occasion, drilling trough the ice cover into large gas pockets has produced geysers that erupt for several days.

SAR imagery and processing. Sentinel-1 Interferometric Wide swath (IW) single-look complex (SLC) imagery were obtained from the European Space Agency. We used acquisitions over Lake Untersee between February 2019 and June 2023, inclusively. Both ascending and descending orbit directions were available in single horizontal co-polarization (HH) giving a 4-year SAR record with a total of 435 acquisitions. The pixel spacing is 3.85 m in slant-range and 14.1 m in track for both trajectories, and the angles of incidence for the center of the lake are 36.7 and

31.5° for ascending and descending trajectories, respectively (lake boundary near and far edge angles are ± 0.1 °).

PCI Geomatics was used for SAR imagery pre-processing. The steps included radiometric calibration to sigma naught quantities, co-registration to one common reference image, multi-looking to reduce speckle and to give 14 m square pixels (1 × 3.6 in track and range, respectively), conversion to the decibel (dB) scale, and orthorectification to UTM Zone 33D using the global 30-m cell size (GLO-30; Copernicus product) digital elevation model. The pre-processed imagery was then used to analyze patterns of backscatter intensity over the lake and to produce time series of backscatter intensity for select locations (**Fig. 5**). For the time series analysis, pixel intensities were averaged over an area of 3 × 3 pixels (42 × 42 m) to smooth spatial variations in pixel values.

Field measurements. The meteorological station along the shoreline of Lake Untersee (612 m asl) was damaged following a glacial outburst flood in January 2019 (Faucher et al., 2021) and a new station was installed in the nearby Aurkjosen Valley (625 m a.s.l). The 2019-2022 mean daily air temperature from the Aurkjosen Valley station was compared with the time series of backscatter intensity, and to infer the freezing period of the ice cover.

In November 2022, water depth and ice cover thickness were measured at 14 borehole sites (**Fig. 5; Supplementary Table 1**). Three boreholes were selected to compare SAR backscatter time series and observations of the presence and morphology of gas bubble from video footage captured under the ice cover in November-December 2022 close to or on the day of scheduled Sentinel-1 flyovers. Sites BH02 and BH03 were selected as they correspond with an area of thick ice (4 m) and thin ice (2.5 m), respectively, and site BH07 was selected as a region of interest during preliminary SAR analysis and has a relatively thick ice cover (3.7 m). The observations under the ice cover were made with a video camera recording 4K, 30 frames per second. All footage was captured with the same viewing angle using a camera rigging apparatus lowered down the borehole. Individual frames were then extracted from the footage at a time when the camera was just below the ice cover looking up at the ice/water interface.

3. Results and Discussion

SAR Backscatter Intensity over Lake Untersee. The 2019-2023 Sentinel-1 SAR record over Lake Untersee reveals two distinct periods during which backscatter intensities were predominantly low or high across the lake. Each year, between December and March (austral summers), backscatter intensities over the entire lake were at their annual minima with an average of –11.6 and –10.0 dB in ascending and descending acquisitions, respectively. Conversely, between May and November, backscatter intensities were at their annual maxima with an average of –4.8 and –3.9 dB in ascending and descending acquisitions, respectively. The difference in backscatter intensity between trajectories (1.6 and 0.9 dB during minima and maxima, respectively) is likely due to the difference in viewing angle: the steeper off-nadir angles of the descending acquisitions are more sensitive to surface roughness compared to the shallower off-nadir angles of ascending acquisitions (i.e., Duguay et al., 2002).

Between the two distinct periods are transitional phases where the intensities change from being predominantly high to predominantly low, or vise versa (**Fig. 6**). The shift from low to high backscatter intensities occurs between April and May, and takes on average 64 days to complete across Lake Untersee. Conversely, the shift from high to low intensities occurs between late November and early December and lasts on average only 20 days. However, at any given location on the lake, the switch between high and low intensities occurs abruptly **(Fig. 7**). For example, between two consecutive ascending acquisitions on 16 and 22 November 2020, site BH03 recorded a sudden drop-off of 14.3 dB (from –3.5 to –17.8 dB), and between two consecutive ascending acquisitions on 8 and 14 May 2020, site BH07 experienced an abrupt increase of 8.1 dB (from –16.2 to –8.1 dB).

The transitional phases show a spatio-temporal pattern of change across the lake. The abrupt increase in intensity observed in April first occurs along the southern and north-eastern shorelines and gradually progressed towards the central region of the lake. The abrupt decreases in intensity observed in late November first occurs in the central regions and gradually progressed towards the shorelines. As such, the duration of the high backscatter period was longest for regions along the shorelines and the duration of the low backscatter period were longest for central regions of the lake. An exception to this general concentric pattern of change in SAR intensity is the area on the south-western side of the peninsula. During each year of the

SAR record, this region displayed low intensities for 1 or 2 months only (December and January) and experienced gradually increasing or high intensities for the rest of the year.

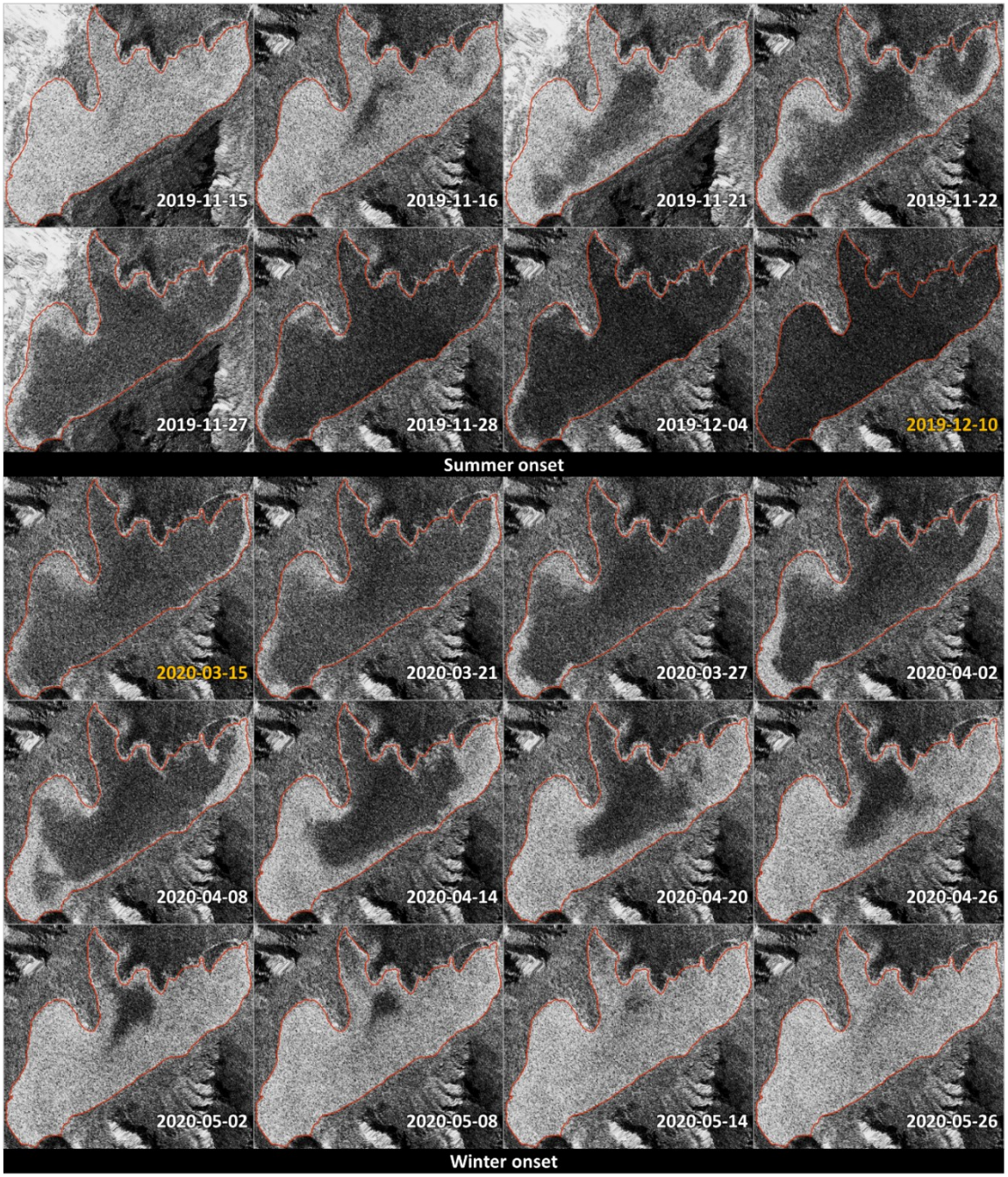

Fig. 6 Patterns of backscatter change over Lake Untersee. Examples of the spatio-temporal patterns of SAR backscatter intensity (dB) change regularly observed over Lake Untersee between seasons during the 4 years of available SAR imagery.

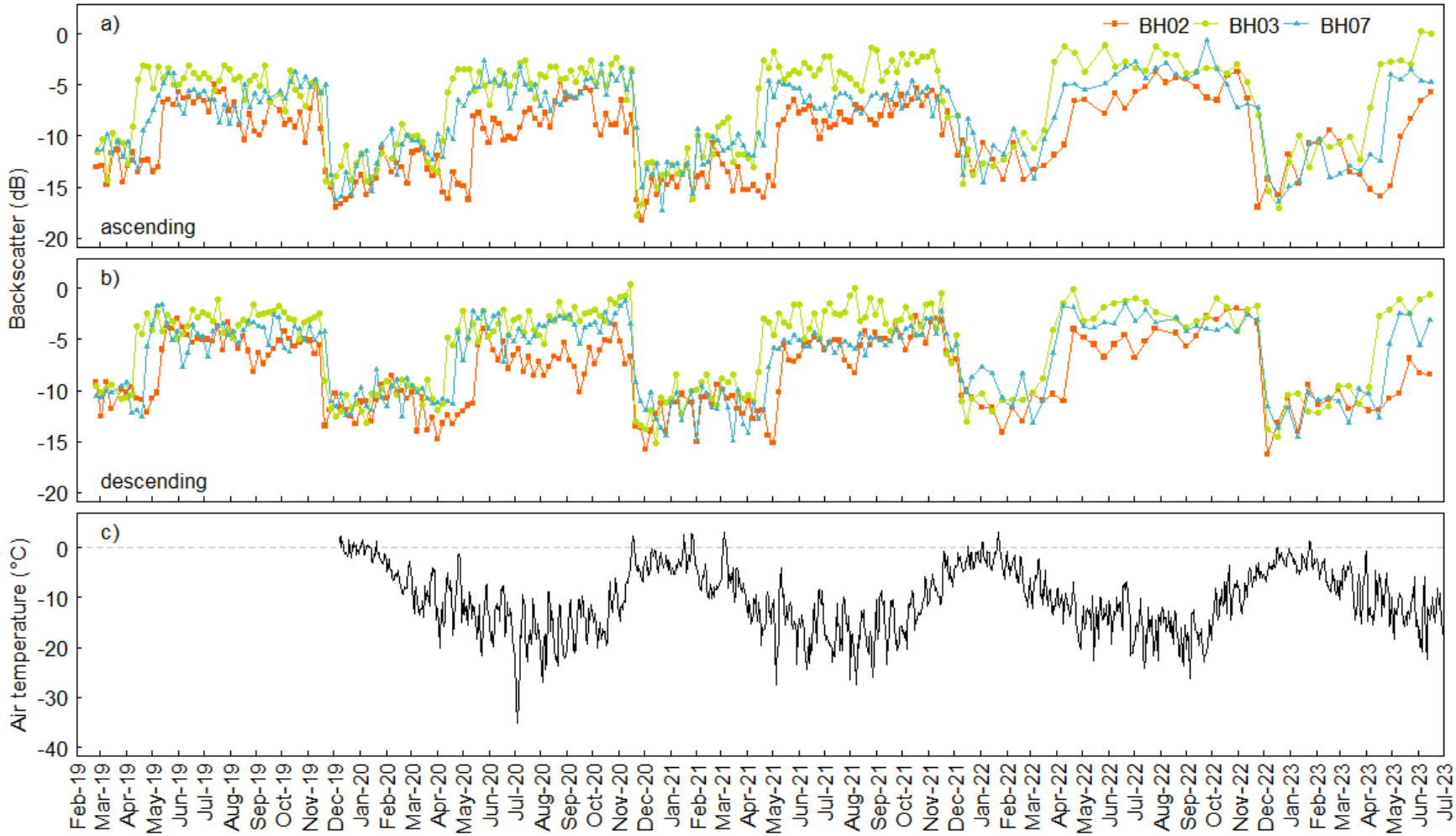

Fig. 7 Time series of SAR backscatter and air temperature. Time series of SAR backscatter (dB) over BH02, BH03, and BH07 between February 2019 and July 2023 for **a)** ascending acquisitions and **b)** descending acquisitions. **c)** is the mean daily air temperature (°C) recorded between December 2019 and June 2023 at the Aurkjosen Valley meteorological station; dashed line is 0 °C.

Several processes have been advanced to explain the temporal changes in backscatter intensity of seasonally ice-covered (SIC) Arctic lakes. First, seasonal changes in backscatter intensity are associated to lake ice phenology; the seasonal onset of freezing and continued ice accretion in winter produce the higher intensities, whereas the melting of the ice cover in spring produce lower intensities (Antonova et al., 2016; Duguay et al., 2002; Murfitt & Duguay, 2020). Additionally, shallow SIC lakes can display sharp drop-offs in intensity if their ice cover reaches the lakebed (e.g., Antonova et al., 2016; Morris et al., 1995). Lake Untersee has a perennial ice cover that floats throughout the year (the ice cover thickness is between 2 and 4 m and the water column is 169 m at its deepest point). Therefore, temporal changes in backscatter intensity associated with lake ice phenology and grounding of the ice cover can both be ruled out. The accumulation of deformation features, such as cracks, are known to increase lake ice backscatter (Morris et al., 1995). Diurnal temperature fluctuations at the beginning of summer cause thermal contraction cracking over the entire ice cover of Lake Untersee, and this cracking slows during the 24-hour daylight period. However, because cracking continues past the period when backscatter switches from high to low, ice cracks cannot explain the season backscatter patterns. Candle ice, a deformational ice property that can develop in seasonal lake ice when individual ice crystals begin to separate during melting (Muguruma & Kikuchi, 1963), does not occur in the Lake Untersee ice cover.

On lake ice, the presence of snow can produce higher backscatter returns (Stiles & Ulaby, 1980; Surdu et al., 2015). As an example, 2-5 cm of snow fell over Lake Untersee on 23-24 November 2021 and the katabatic winds redistributed some of the snow to the north-west sector (**Supplementary Note 1, Supplementary Fig. 1**). Although the snow produced higher intensities in that area with values comparable to the high backscatter period (**Supplementary Fig. 2**), the snow was present only for a few days to weeks (depending on location) and the patterns of snow redistribution across the lake was inconsistent with the concentric pattern of seasonal backscatter change. Additionally, optical satellite imagery shows the ice cover to be largely free of snow between September and March (**Supplementary Note 2**), meaning that the presence of snow can be ruled out as a possible mechanism for the seasonal change in backscatter intensities. As such, the most commonly accepted mechanisms proposed to explain the seasonal variability of backscatter intensity for Arctic lakes do not apply to the observed seasonal variability of backscatter intensity for Lake Untersee.

Dynamic roughness at the ice/water interface drives seasonal change in backscatter intensity. We propose, based on Gunn et al. (2018), that gas bubbles at the ice/water interface of Lake Untersee create enough roughness to eclipse C-band microwaves and produce a strong backscatter response. This is consistent with the recent discoveries that single bounce at the ice/water interface is the dominant scattering mechanism from floating lake ice despite the presence of vertically oriented bubbles in the ice cover (Atwood et al., 2015; Gunn et al., 2018), as well as with numerical simulations that ice/water interface roughness has the largest contribution to the backscatter response of floating lake ice (Murfitt et al., 2022, 2023). However, unlike Gunn et al. (2018) who considered bubbles at the interface to remain static, we propose that changes in radiometric roughness associated with bubbles at the ice/water interface is seasonally dynamic and is the main driver for the seasonal patterns in backscatter intensity observed over Lake Untersee.

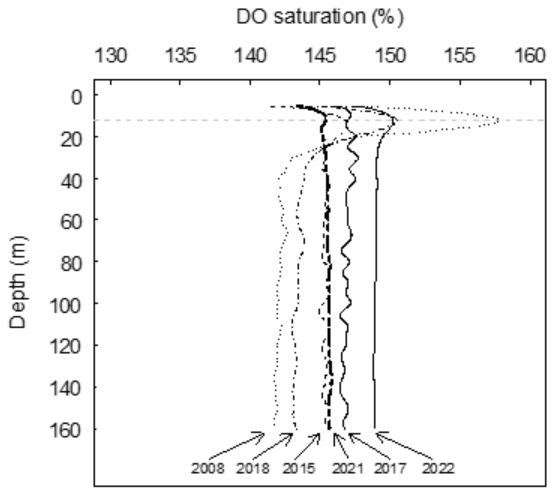

Fig. 8 Dissolved oxygen (DO) profiles of the Lake Untersee water column. The saturation of DO in the lake basin was recorded annually between 2008 and 2022 in November/December. At this time of year, the saturation of DO is around 140-150 %, but can be elevated by c. 12 % near the surface, around 12 m depth (dashed horizontal line).

Lake Untersee, like many other Antarctic PIC lakes, is supersaturated in dissolved gases (Andersen et al., 1998; Craig et al., 1992; Wharton et al., 1987). As gases exsolve from water freezing at the ice-water interface and accumulate in the boundary layer, bubble nucleation can occur once a critical saturation threshold is reached (Andersen et al., 1998; Lipp et al., 1987; Yoshimura et al., 2008). Profiles of DO from Lake Untersee are here used to infer seasonal

differences in gas saturation near the boundary layer. The saturation of DO in Lake Untersee averages 150 %, but profiles measured in mid-November to early-December are different to those from January and February. The profiles from November-December show that DO can increase by more than 12 % around 15 m depth compared to the rest of the water column (**Fig. 8**), whereas in January and February, the DO profiles remain flat throughout the water column (Wand et al., 1997, 2006). As such, the exsolved gas during the freezing period, which would occur during the colder months, would likely produce the increased DO supersaturation just below the ice cover. Conversely, little to no active freezing would take place during the warmer summer period, allowing the exsolved gases to mix in the water column, which likely occurs on a monthly timescale in Lake Untersee (Steel et al., 2015).

Video footage captured below the ice cover at three locations of Lake Untersee (BH02, BH03, and BH07) on dates close to SAR imagery acquisition was used to verify the presence of gas bubbles and their effect on backscatter intensity. In footage captured prior to and on 22 November 2022, gas bubbles were present in abundance below the ice cover at all three sites. The footage showed that a layer of densely packed bubbles completely covered the ice/water interface within the field of view (**Fig. 9**). Conversely, in footage captured on and after 25 November 2022, the abundance of small gas bubbles at all three sites was reduced; the footage showed bubbles that were more distantly separated. The lower abundance of bubbles also made it possible to observe the ice underside, which appeared to be smooth with no large-scale undulations or pits, a phenomenon that can occur when the insulating effects of large gas bubbles limit the accretion of ice (Engram et al., 2012, 2013b). These observed changes in the abundance of bubbles appear to be temporally correlated with the abrupt decrease in backscatter intensity recorded at the three sites between 23 and 24 November 2022. Prior to 23 November 2022, the three sites had high backscatter intensities (–3.4, –1.8, and –3.1 dB for BH02, BH03, and BH07, respectively), typical of the period between May and November. However, on and after 24 November 2022, the three sites experienced a substantial decrease in backscatter intensity (–17.0, –8.0, and –7.2 dB for BH02, BH03, and BH07, respectively) and remained at low values typical of the intensities seen between December and March. These observations indicate that the abundance of bubbles at the ice/water interface affect the backscatter intensity over Lake Untersee.

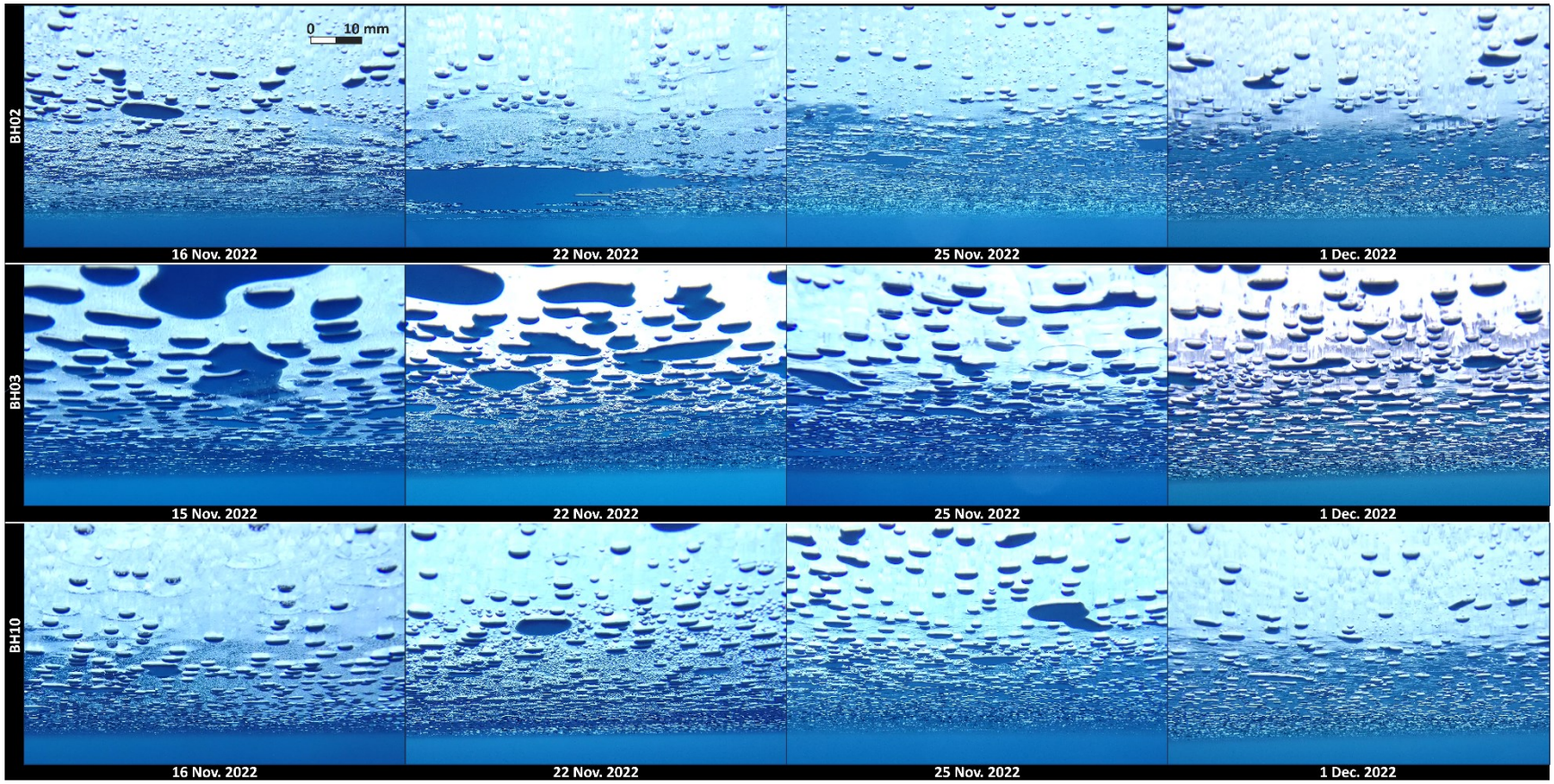

Fig. 9 Bubbles under the ice cover of Lake Untersee. Frames extracted from video footage captured under the ice cover at sites BH02, BH03, and BH7 between mid November and early December 2022. Photos taken by A. Gaudreau using a submersible video camera attached to a rope. Note, the scale bar is only accurate for features at the top of the frames.

The development and increased abundance of gas bubbles at the ice/water interface would take place during the freezing period, which would occur during the colder months when the temperature of the ice/water interface is sufficiently cold. Adams et al. (1998) showed that the thermal response of a perennial ice cover at 1, 2 and 3.5 m ice depths is lagged by c. 50, 100 and 140 days, respectively, following the time when surface air temperatures were consistently below 0 °C. In the Lake Untersee ice cover where ice thickness ranges between c. 2 and 4 m, similar lags in the timing of thermal response can be expected, meaning the onset and length of freezing period at the ice/water interface would relate to the ice thickness. The SAR time series show that intensity values at the three sites are related to air temperatures recorded at the Aurkjosen Valley meteorological station (**Fig. 5**): intensities are low when air temperatures are above c. –4 °C, and intensities are high when air temperatures are below c. –4 °C. As an estimate of the freezing period for Lake Untersee, we used the mean daily air temperature between 2008 and 2023 to compute the thermal gradient through a 2.8 m thick ice cover (**Fig. 10**). As a first order estimate, the freezing period is taken as the period when the daily thermal gradient is lower than the mean annual thermal gradient. This suggests that freezing would take place between April and November and corresponds roughly to the timing of abrupt changes in backscatter intensities.

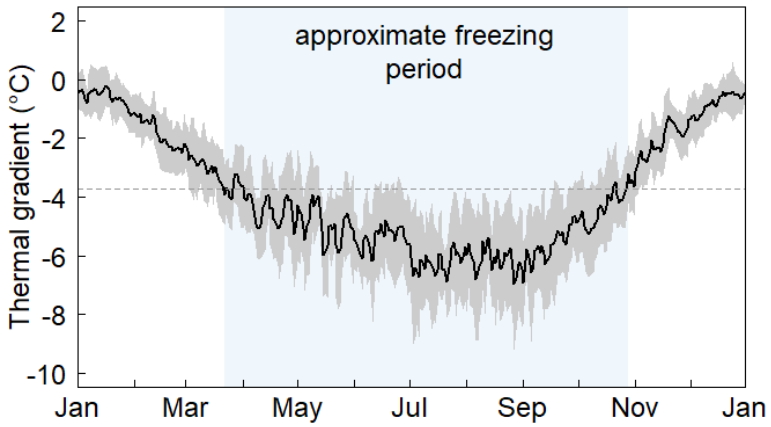

Fig. 10 Approximate freezing period of the Lake Untersee ice cover. Average daily thermal gradient (black line) for the Lake Untersee ice cover between 2008 and 2023 between surface air temperature and the ice/water interface (0 °C) for an average ice thickness of 2.8 m. The grey area is ± 1 standard deviation, the dashed line is the all-time average thermal gradient, and the blue area is the period when the daily gradient is below the all-time average gradient.

Ice/water interface bubble morphology and roughness. Contrary to the hypothesis that attributed high backscatter to a double bounce interaction between the ice/water interface and vertically oriented bubbles within the ice cover, Gunn et al. (2018) suggested that bubbles at the ice/water interface of a floating lake ice cover create the necessary roughness to exceed the RMS height threshold of C-band wavelengths and produce backscatter. Our footage within and below the ice cover supports the findings of Gunn et al. (2018). Cores collected from the ice cover of Lake Untersee showed that it contains bubbles of various morphologies (spherical, oval, dendritic, and tubular), at times occupying as much as 50 %vol (Faucher et al., 2019). Lowering the video camera down the boreholes also showed long tubular bubbles c. 10 to 100 cm in length distributed in the ice cover at the 3 sites during the period of low backscatter (**Fig A3.1**). The footage also revealed that bubbles were present in abundance at the ice/water interface prior to 25 November during the period of high backscatter. The majority of the bubbles at the interface were circular with a diameter of c. 1 cm or less, but many large gas pockets tens of centimeters to several meters in diameter were also present. The smaller circular bubbles were observed at the ice underside at the terminus of overhead bubbles as well as on the flat and smooth ice surface between overhead bubbles, signifying recent nucleation or bubble growth with little ice growth. Although a range of bubble shapes were observed, all bubbles and gas pockets extended from the ice underside by c. 5 mm or less. Bubbles larger than c. 5 mm in diameter were not dome-shaped but flatter due to the large hydrostatic pressures which push gas up against the ice underside.

The bubbles that were observed at the ice/water interface satisfy the condition for surface roughness at C-band wavelengths according to the Fraunhofer criterion:

$$s < \frac{\lambda}{32 \cos\theta} \tag{11}$$

where surfaces with RMS height deviations that meet s are considered smooth and specular with respect to the incident wavelength λ for a given angle of incidence θ. Because this criterion assumes in situ wavelength, the sensor wavelength must be adjusted to account for to the relative permittivity ε' of the propagation material (ice):

$$\lambda = \frac{1}{\sqrt{\varepsilon'}} \frac{c}{f} \tag{12}$$

where c is the speed of light in a vacuum in m s^{-1} and f is the system frequency in Hz. We also account for the refracted angle of wave propagation following wave penetration into ice with Snell's law:

$$n_1 \sin \theta_1 = n_2 \sin \theta_2 \quad (13)$$

where n is the refractive index given with $\sqrt{\varepsilon'}$ and the subscripts 1 and 2 denote the media the wave travels from and to, respectively.

From these calculations, we obtain a shortened wavelength of 3.12 cm and shallower propagation angles of 19.8 and 17.3 ° for ascending and descending acquisitions, respectively, after penetrating pure ice with a ε' = 3.17. The actual average ε' for the Lake Untersee ice cover is closer to 3.09 due to its high bubble content, but this would not greatly affect the final wavelength. For Sentinel-1 with f = 5.405 GHz, we obtain a RMS height threshold of 1.03 mm in both trajectories for the ice/water interface to be considered rough and capable of producing backward reflections. The dense and widespread coverage of bubbles at the ice/water interface with heights of c. 5 mm, such as those observed prior to 25 November, likely provide sufficient height variations to exceed the RMS height threshold. Therefore, it is likely that the relatively small bubbles c. 1 cm in diameter or less at the underside of the ice cover of Lake Untersee are the dominant scattering source and their abundance provide the mechanism of the seasonal change in backscatter intensity. On the other hand, large bubbles c. 1 cm in diameter or more, gas pockets several meters in diameter, and the greater proportion of smooth ice surface, such as those observed on and after 25 November, would reduce backscatter as their relatively flat surfaces are akin to an interface of air and calm water, or a smooth ice/water interface, reducing the RMS height deviations, leading to specular reflections away from the antenna (**Fig. A3.2**).

Spatio-temporal variations in backscatter intensities over Lake Untersee. The main driver for the variations in backscatter intensities over Lake Untersee is likely related to the abundance of < c. 1 cm diameter bubbles at the ice/water interface: high backscatter occurs during the cold season when water freezes to the ice underside, gases exsolve, and nucleation and growth of bubbles takes place, whereas low backscatter occurs during the warm season when no freezing takes place and bubbles are either dissolved into solution or coalesce to form larger ones. However, the concentric pattern of backscatter intensity change that occurs between these two periods suggests that the period of freezing, gas exsolution, and bubble abundance is not uniform

across the underside the ice cover of Lake Untersee. Below, we explore possible mechanisms for the spatial pattern observed during the switch in intensities.

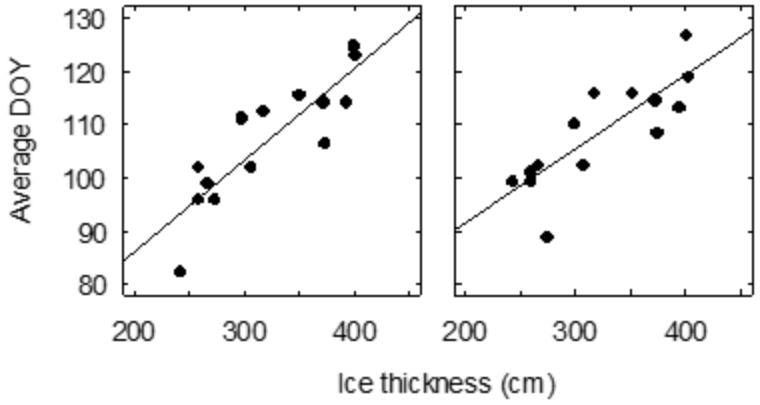

Fig. 11 Relationship between the timing of backscatter change and ice thickness. Average day-of-year (DOY) of backscatter increase during the 4 years of SAR record at n=14 boreholes as a function of ice thickness (cm) for the ascending trajectory (left) and descending trajectory (right).

The duration of the freezing period below the ice would be affected by the thickness of the ice cover, which varies between 1.9 and 3.9 m around the lake (Faucher et al., 2019). From the SAR imagery, we observed that the switch from low to high intensities in April/May occurs earlier where the ice cover is thinner and up to 78 days later where the ice cover is thicker (**Fig. A3.3**). In fact, the thickness of the ice cover is positively correlated with the average day-of-year (DOY) of the abrupt increase in backscatter intensity at the 14 boreholes during the 2019-2023 SAR record; Pearson's correlation coefficients are 0.87 and 0.82 (p-values < 0.05) for the ascending and descending trajectories, respectively (**Fig. 11**). However, no statistically significant correlation was found between the average DOY of the abrupt decrease in backscatter intensity and ice cover thickness (Pearson's correlation coefficients of –0.32 and 0.30 in ascending and descending, respectively).

The above correlations suggest that the variations of ice thickness have a key role in the timing of change from low to high intensities and are less important during the change from high to low.

The early summer abrupt decrease of intensities occurs during a period when gas saturation at the ice/water interface is higher following the freezing period (i.e., the c. 12 % increase of DO around 15 m depth), thus the poor correlation with ice thickness could relate to the monthly timescale lag in mixing of the water column, a process that occurs independent of

ice thickness. Conversely, the late summer abrupt increase in intensities occurs when dissolved gases are well-mixed in the water column. The variations in ice thickness are known to cause substantial differences in the rates of ice accretion (i.e., Faucher et al., 2019) which would ultimately affect the rates of gas accumulation in the boundary layer (Carte, 1961; Lipp et al., 1987). Thus, the onset of freezing which progresses radially inward from thinner ice to thicker ice initiates the process of gas exsolution and bubble nucleation in a similar radial pattern. Additionally, the variations of ice thickness across the lake would be associated with variations of pressure below the ice. Because dissolved gas saturation is affected by pressure, among other factors, variations in hydrostatic pressure below the ice likely also affect the critical nucleation saturation of bubbles (Andersen et al., 1998) and the timing of nucleation. However, the timing of backscatter increase is likely not only affected by ice thickness. For example, the area behind the peninsula has relatively thick ice (c. 3.5 to 4 m) and displays high intensities during much of the year. In models of water column circulation, the bay area had among the slowest circulation velocities because it is shielded by the peninsula (Steel et al., 2015). Additionally, the bathymetry of the bay area is characterized by a large expanse of relatively shallow water c. 20 to 40 m in depth (Wand et al., 2006). Thus, poor circulation in conjunction with shallow waters likely allows dissolved gases to accumulate more rapidly, ultimately leading to earlier bubble nucleation. This might also explain why ice in the bay area is characterized as under dense (i.e., Faucher et al., 2019).

Comparison with other ice covers. Antarctica hosts numerous PIC lakes (Doran et al., 2007; Priscu et al., 1998; Vincent & Laybourn-Parry, 2008), and preliminary analyses indicates that several experience similar seasonal backscatter regimes as Lake Untersee (**Fig. 12, Supplementary Note 3**). The perennial ice covers of Lake Obersee in the Untersee Oasis and Lake Vanda and Lake Fryxell in the McMurdo Dry Valleys (MDV) have seasonal backscatter regimes that are similar to those observed over Lake Untersee; winter intensities are high while summer intensities are low. Lake Untersee and Lake Obersee are categorically similar, meaning similar sub-aqueous process responsible for backscatter variations likely operate in both lakes. In contrast, Lake Vanda and Lake Fryxell experience summer moating which is expected to account for significant gas losses (Craig et al., 1992). Additionally, Lake Vanda experiences greater summer moating. Therefore, the difference in backscatter intensities between the MDV and

Untersee Oasis PIC lakes likely relates to the seasonal accumulation and loss regimes of gases in their basins and their impacts on the abundance of bubbles at their ice/water interface. In comparison, the seasonality of backscatter intensities observed over the seasonal ice cover of Lake Hazen in the high Arctic, for example, or over sea ice, can be attributed to surficial processes such as specular scatter from calm water, Bragg scattering from waves, and specular reflection from a smooth ice/water interface, or processes that affect the structural composition of the ice, such as snow-ice, cracks and deformation features, refrozen pond water, and bubbled internal layers (Murfitt & Duguay, 2020). Ice/water interface bubbles likely have a smaller contribution because SIC lakes typically have a summer ice-off period when winter accumulations of dissolved gases can escape to the atmosphere. Thus, fresh and smooth FY ice, having relatively few deformation features or heavily bubbled internal layers, have relatively low backscatter intensities. Once FY ice endures a period of decay and deformation and is reclassified a MY ice, like sea ice or the MY ice observed over Lake Hazen in winter 2022/2023, backscatter intensities can approach or even surpass peak intensities recorded over well-sealed PIC lakes during a period when there is a high abundance of bubbles at their ice/water interface.

Implications for future studies. Over Lake Untersee, it was found that the abrupt changes in backscatter intensity relate to the abundance of small bubbles at the ice/water interface, which is spatially correlated with variations in ice thickness. These variations in ice thickness, in turn, affect the rate of freezing and gas rejection at the ice/water interface. This is corroborated by a comparison with other PIC Antarctic lakes that also experience seasonal gas buildup. Furthermore, this comparison highlights the importance of conducting comparative backscatter analyses between well-sealed and moat-forming PIC, as the latter may serve as analogues to the former in future climate warming scenarios. A comprehensive examination of the impacts of seasonally-dynamic dissolved gases and interface bubbles on backscatter intensities in both PIC and SIC lakes is warranted. However, the opportunity to better understand the unique backscatter phenomenon of Lake Untersee and Lake Obersee, characterized by their well-sealed ice covers that do not experience seasonal moating or degassing, is threatened by climate warming.

Our findings could also serve as an analogue for the Europa Clipper mission. Europa is one of Jupiter's icy moons suspected to have a liquid water ocean beneath its icy shell. The REASON instrument (a radar profiler) aboard Europa Clipper could reveal possible clues into

the dynamics of gas and bubble nucleation at the ice/water interface which may have important scientific implications for the internal structure of ice and the search of extraterrestrial life.

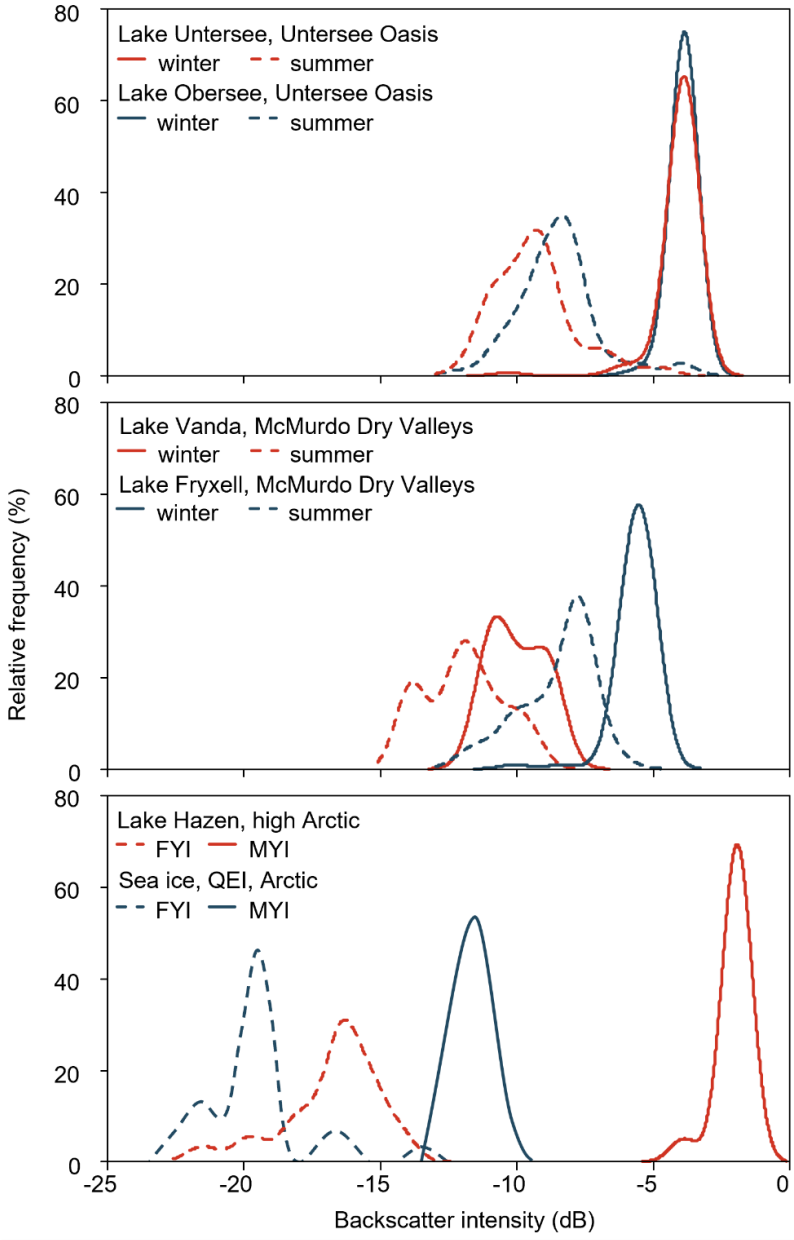

Fig. 12 Frequency distribution of backscatter over ice covers. Frequency distribution of backscatter intensity (dB) between February 2019 and June 2023 over Lake Untersee, Lake Obersee, Lake Vanda, and Lake Fryxell for winter (April to October) and summer (November to March), over Lake Hazen first-year ice (FYI) (October to May) and multi-year ice (MYI) (October 2022 and June 2023). The distributions for sea ice are from Mahmud et al. (2020) derived from RADARSAT-2 imagery over the Queen Elizabeth Islands (QEI), Canada for the months November-December, January-May in 2009.

Data availability

- The Sentinel-1 synthetic aperture radar (SAR) datasets are courtesy of the European Space Agency (ESA) Copernicus program and are available from the Copernicus Open Access Hub [https://scihub.copernicus.eu/] as well as from the Alaska Satellite Facility (ASF) Vertex web platform [https://asf.alaska.edu/]
- The video footage and/or video footage frames used for ice/water interface observations are available from the corresponding author upon reasonable request.

Acknowledgements

This work was made possible by the Antarctic Logistics Centre International, Cape Town, South Africa, and the Arctic and Antarctic Research Institute/Russian Antarctic Expedition. We are grateful to Colonel (I.L.) J. N. Pritzker, IL ARNG (retired), Lorne Trottier, and fellow field team members for their support during the expeditions.

Funding:

TAWANI Foundation (DA)
Trottier Family Foundation (DA)
Canadian Space Agency FAST grant (DL)
NSERC Discovery Grant (DL)
NASA Exobiology (DA)

Author contributions

A.G. collected field data, SAR imagery, and performed the analyses. A.G. developed the theories and was the lead researcher and writer. D.L. proposed the DOY backscatter change /ice thickness analysis and contributed to the interpretation of results. A.G. and D.L. were lead manuscript editors. D.A. contributed feedback to the interpretations and helped with manuscript editing.

Competing interests

All authors declare no competing interests.

Supplementary information

- Supplementary Table 1
- Supplementary Note 1
- Supplementary Fig. 1
- Supplementary Fig. 2
- Supplementary Note 2
- Supplementary Note 3

4. References

All references in this document are presented immediately following Chapter 4.

Chapter 3: Supplementary information and special features

1. Introduction

The primary findings of this research were presented in Chapter 2 in the format of a journal manuscript, thereby facilitating the dissemination of the results to the broader academic community. However, numerous supplementary findings, while pertinent to the research objectives, were not presented within the confines of the journal manuscript. This chapter expands upon the scope of the journal manuscript to enrich the overall understanding of backscatter over lake ice.

In Chapter 2, the seasonal backscatter frequency distribution of other PIC lakes in Antarctica, first-year (FY) and multi-year (MY) Arctic lake ice and sea ice was presented and placed into a broader context with backscatter observed over Lake Untersee. This chapter presents the backscatter time series of the lakes: the well-sealed, non-moat forming PIC lakes in the Untersee Oasis (Lake Untersee and Lake Obersee), moat-forming PIC lakes in the McMurdo Dry Valleys (Lake Vanda and Lake Fryxell), and the FY and MY ice of a seasonally ice-covered (SIC) Arctic lake (Lake Hazen). A brief description of these additional lakes is given in order to place the backscatter regimes in the context of basin characteristics. Lastly, this chapter presents and analyzes distinctive and unusual backscatter features observed over Lake Untersee and Lake Obersee. The methods used to acquire and process the imagery for all supplementary lakes in this section are the same as described in the Methods sections of the manuscript. All time series comparisons are made using the descending trajectory acquisitions of Sentinel-1 for the same period used in the journal manuscript.

2. Comparison of ice-covered lakes

2.1. Lake Untersee and Lake Obersee, Untersee Oasis, Antarctica

Chapter 2 presented the SAR backscatter of Lake Obersee in detail. Here, the SAR time series of the nearby Lake Obersee is presented. Lake Obersee is a relatively small ice-dammed lake located 7 km north-east of Lake Untersee (**Fig. 4**). The lake is c. 2.7 km wide by 2.6 km long, has a surface area of 3.4 km^2, has an ice thickness of 3.5 to 4 m, and a maximum water depth of c. 55 m (Schwab, 1998) or c. 44 m after a recent drainage event (Faucher et al., 2021). Lake

Obersee is dammed by the Vangengejma Glacier to the north and the Obersee Glacier to the south; sub-aqueous melt from these glaciers is the primary sources of water recharge for Lake Obersee. Like Untersee, the Lake Obersee basin is well-sealed by its perennial ice cover, resulting in water column DO supersaturation around 150 %. Lake Obersee has higher levels of dissolved nutrients and greater primary productivity compared to Lake Untersee (Faucher et al., 2021).

Both lakes have very similar backscatter intensity time series (**Fig. 13**). Summer (November to March) intensities are –9.4 and –8.5 dB and winter (c. April to October) intensities are –4.0 and –3.9 dB for Lake Untersee and Lake Obersee, respectively. In fact, their time series have a Pearson's correlation coefficient of 0.96. This high degree of correlation is shown both in their seasonal oscillations which are matched almost identically, and in the intra-seasonal variability. For example, with the exception of the 2021-2022 summer period, the small intensity variations during summers are almost perfectly mimicked between both lakes. The poor correlation during the 2021-2022 summer period is likely due to the partial covering of snow following the snow fall events in November 2021 (see **Appendix 1: Supplementary information to the journal manuscript – Supplementary Note 1: Effects of snow on Lake Untersee backscatter intensities**). The high degree of correlation between the Lake Obersee and Lake Untersee backscatter time series suggests the same or similar processes responsible for backscatter intensity variations operate in both lakes.

2.2. Lake Vanda and Lake Fryxell, McMurdo Dry Valleys, Antarctica

The McMurdo Dry Valleys (MDV), situated in Victoria Land west of McMurdo Sound, are known for their extreme polar aridity and unique geological features. The MDV host numerous large ice-covered lakes and ponds which harbour life in one of the most extreme and challenging environments on Earth (Doran et al., 2008; Vincent & Laybourn-Parry, 2008). These bodies of water exist in a region characterized by severe cold and aridity, where temperatures frequently drop below –40 °C, and precipitation is exceedingly scarce. Thus, their primary source of replenishment is the surface melt runoff streams of nearby glaciers (Doran et al., 2008).

Lake Vanda is a PIC lake located in Wright Valley (77.53S, 161.57E) and is home to a diverse microbial community in the form of elaborate microbial pinnacles and mats that line the lake floor (Sumner et al., 2016). The lake is c. 7.5 km long by 1.5 km wide, has a surface area of

7.5 km^2, an ice thickness of 3.5-4 m, a maximum water depth of at least 74 m, and develops a moat during the summer (Schutte et al., 2020). The mean annual air temperature recorded near Lake Vanda between 1994 and 2017 is –19.5 °C (Obryk et al., 2020). The Lake Vanda basin is recharged by the Onyx River which flows for 30 km inland from the Lower Wright Glacier. Water entering Lake Vanda is air saturated, and the near-surface water layers become supersaturated in winter through the process of freeze enrichment (Andersen et al., 1998).

Lake Fryxell is a PIC lake located in Taylor Valley (77.61S, 163.16E). The lake is c. 5.5 km long by 1.7 km wide, has a surface area of 6.7 km^2, an average ice thickness of 5 m (Hood et al., 1998), and a maximum water depth of 18 m (Lawrence & Hendy, 1985). The mean annual air temperature recorded near Lake Fryxell between 1987 and 2017 is –20.0 °C (Obryk et al., 2020). The Lake Fryxell basin is recharged primarily by a run-off stream originating at the Canada Glacier as well as by numerous surrounding inflowing streams (Doran et al., 2008). Gases near the ice/water interface of Lake Fryxell become supersaturated with respect to atmospheric equilibrium from freeze enrichment (Hood et al., 1998).

Backscatter intensities over the Lake Vanda and Lake Fryxell ice covers show seasonal backscatter regimes (**Fig. 13**). Although less synchronized, similar seasonal backscatter features are observed between these two lakes; their time series have a Pearson's correlation coefficient of 0.67. This suggests both lakes have unique components that influence their backscatter intensities. The seasonal oscillations are more pronounced over Lake Fryxell, and intensities are on average 4.0 dB higher over Lake Fryxell. Summer (c. November to March) intensities are –12.0 and –8.5 dB and winter (c. April to October) intensities are –10.0 and –5.6 dB for Lake Vanda and Lake Fryxell, respectively. Both lakes experience sharp increases and decreases at the onset of the seasons; sharp winter increases are more pronounced over Lake Vanda while sharp summer drop-offs are more pronounced over Lake Fryxell. Both lakes experience progressively decreasing backscatter intensities throughout the winter season; intensities over Lake Vanda fluctuate during the winter decline while Lake Fryxell experiences relatively little winter declining fluctuations.

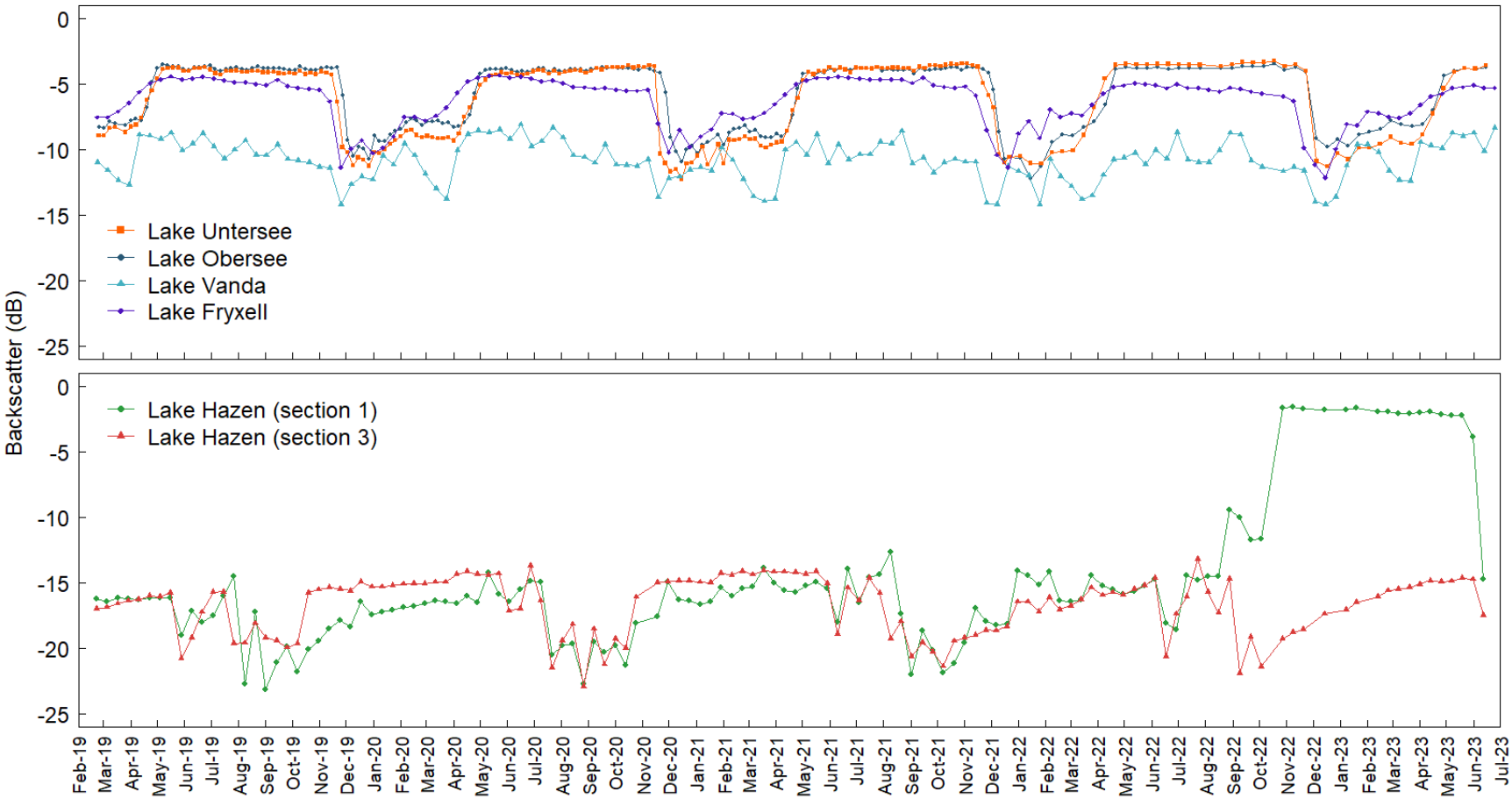

Fig. 13 Comparison of time series of SAR backscatter over lake ice. Time series of SAR backscatter (dB) over Lake Untersee, Lake Obersee, Lake Vanda, and Lake Fryxell (top) and two sections of Lake Hazen (bottom) between February 2019 and July 2023 in the descending trajectory. Delineations of sections 1 and 3 are the same as in **Murfitt & Duguay (2020)**.

2.3. Lake Hazen, high Arctic Canada

Lake Hazen is the largest freshwater lake in the high Arctic, located on Ellesmere Island, Nunavut, Canada (81.78N, 71.20W). The lake is c. 70 km long by 10 km wide, has a surface area of 542 km^2, a maximum water depth of 267 m (Köck et al., 2012; Obryk et al., 2020), and is recharged primarily by glacial run-off streams. Climate normals between 1981 and 2010 from the Alert weather station located 150 km north of Lake Hazen show daily average air temperatures of 3.4 °C in July and –33.2 °C in February (Environment and Climate Change Canada, 2023). Lake Hazen can be considered a quasi-SIC lake in that parts of its surface can remain covered by ice year-round (see **Appendix 2: Multi-year ice over Lake Hazen**), although full ice-off has become a more common occurrence in recent decades (Lehnherr et al., 2018).

Because Lake Hazen was partially covered by MY ice during the period of observation, backscatter time series are here summarized for two contrasting sections of the lake (section 1 and section 3, same as in Murfitt & Duguay, 2020). As shown in Murfitt and Duguay (2020), Lake Hazen experiences regular seasonal oscillations of backscatter, with low (c. –23 dB) and fluctuating intensities coinciding with the warmer ice break-up and ice-off periods, and increasing, high (c. –15 dB), and stable intensities coinciding with the colder ice build-up and ice-on periods (Murfitt & Duguay, 2020). However, between October 2022 and June 2023, sections 1 of the ice cover (**Fig. A2.1**) was covered by MY ice, and a sharp increase of intensities was observed in that area. Average intensities over FY ice (section 3) between October and May are –15.9 dB and average intensities over MY ice (section 1) between October 2022 and June 2023 are –2.0 dB.

2.4. Discussion: Lake comparison

The Antarctic lakes have synchronized backscatter time series; intensities are generally high during winter and low during summer. Their commonality over such a large distance (c. 3350 km) is the hemispheric climate which affects their freezing period. Furthermore, the periods of high and low backscatter between the southern and northern hemisphere lakes are out of phase, reflecting apposing seasons between the hemispheres. This confirms the oscillations are indeed a seasonal response of backscatter intensity. Lake Untersee and Lake Obersee generally have the highest backscatter intensities of all other lakes compared but were surpassed by the MY ice observed over section 1 of Lake Hazen in winter 2022/2023.

The differences in intensities between Lake Vanda and Lake Fryxell are likely related to the seasonal dynamics of dissolved gases just below their ice covers and in their water columns. In Chapter 2, it was suggested that variabilities in water column dissolved gases in Lake Untersee affect the abundance of bubbles below the ice cover, which in turn affect the C-band backscatter intensity. In addition to variable ice freezing rates, water column circulation, and basin depth/volume which impact the dissolved gas regime, summer moating is expected to account for substantial gas loss from PIC lake basins (Craig et al., 1992). Although both Lake Vanda and Lake Fryxell experience summer moating, the SAR imagery over Lake Vanda regularly showed between 100 to 400 m of moat water along segments of the lake perimeter during the summer months. Summer moating at Lake Fryxell was relatively limited; only parts of the lake perimeter had moating of c. 20 to 40 m with only localized regions extending beyond 60 m. Thus, the greater extent of moating of the Lake Vanda ice cover would likely allow for greater gas losses. Additionally, degassing of Lake Vanda would be accelerated by periods of open water (**Fig. A3.1**) from wind-generated mixing, as well as by the convective cells in the lake (Castendyk et al., 2016). Conversely, based on water chemistry analysis, Hood et al. (1998) suggest that upper layers of enhanced dissolved gases in Lake Fryxell are unlikely to experience significant mixing throughout the year, meaning a layer of gas supersaturated water likely remains stagnant just below the ice cover. Thus, with the onset of winter freezing, it is likely that the near-surface layer of water below the Lake Fryxell ice cover becomes critically supersaturated in dissolved gases more rapidly than Lake Vanda, leading to earlier bubble formation with greater abundance and larger size (Carte, 1961), thus resulting in earlier onset of increased backscatter with overall higher intensity values.

The Untersee Oasis lakes and Lake Fryxell initially have similar backscatter intensities at the beginning of the winter seasons (–4 and –4.6 dB, respectively), suggesting that the abundance of bubbles below their ice covers is similar at this time. However, as winters progress, intensities over Lake Fryxell slowly decrease (average intensities are –5.8 dB at the end of winter before drop-off), while intensities over Lake Untersee and Lake Obersee remain relatively unchanged. The Lake Fryxell basin is relatively shallow and has a more gradual bathymetric slope (Lawrence & Hendy, 1985) compared to the bathymetry of Lake Untersee and Lake Obersee (Schwab, 1998). Thus, the declining intensities over Lake Fryxell may in part be due to the gradual grounding of parts of the ice cover (particularly along near-shore segments) as the ice

thickens through winter (**Fig A3.2**), reducing the dielectric contrast. Conversely, no seasonal grounding was observed over Lake Untersee or Lake Obersee during the study period. Furthermore, the shallower basin, in conjunction with minimal mixing, likely results in water at the ice/water interface of Lake Fryxell to reach critical supersaturation more rapidly than the Untersee Oasis lakes with the onset of winter. This may explain why intensities over Lake Fryxell during summer months are similar or higher than over the Untersee Oasis lakes and increase earlier with the onset of winter.

The moating characteristics of MDV lakes and the resulting backscatter intensities serve as important analogues for non-moat forming PIC lakes in future moating scenarios. The mean annual air temperature of the Untersee Oasis (–9.5 °C ± 0.7 °C) (Andersen et al., 2015; Faucher et al., 2019) is relatively warm compared to that of the MDV (c. –20 °C) (Obryk et al., 2020). However, the MDV lakes experience summer moating while the Untersee Oasis lakes remain well sealed year-round; the latent heat of cooling associated with intense surface sublimation (Hoffman et al., 2008) cools their ice covers such that summer moating does not occur. Thus, if air temperatures warm sufficiently or if solar irradiance dominates over sublimation cooling and summer moats begin to develop such that degassing can occur, their future backscatter responses may resemble those recorded over MDV lakes. Additionally, because the Lake Untersee basins more closely resemble that of Lake Vanda in terms of its depth and water column circulation, its backscatter intensities in a moating scenario would likely more closely resemble intensities recorded over Lake Vanda, although a winter declining trend would likely not be observed.

Backscatter intensity variations over PIC lakes in the Untersee Oasis and MDV can largely be attributed to processes that affect the abundance of gases, and therefore bubbles, below their ice covers. Conversely, bubbles are likely not supported in great abundance below the ice cover of Lake Hazen. In c. May, around the time of maximum intensities over Lake Hazen, dissolved gases just below the ice cover can surpass atmospheric saturation, but likely remain below 110 % (in the case of DO) (St. Pierre et al., 2019). Seasonal backscatter intensity variations over the ice cover of Lake Hazen are likely dominated by surficial processes, such as specular scatter from calm water, Bragg scattering from waves, specular reflections from a smooth ice/water interface, and multiple and volumetric scattering from snow-ice, cracks, and deformation features (Murfitt & Duguay, 2020).

Between October 2022 and June 2023, very high intensities of c. –2 dB were recorded over section 1 of Lake Hazen, surpassing intensities recorded over the Untersee Oasis lakes. Bright MY ice covering much of the lake surface can be observed in the SAR imagery during this period (**Appendix 2: Multi-year ice over Lake Hazen**). Characterizations of the structural composition of freshwater MY ice are uncommon. However, MY sea ice, having survived at least one summer melt and decay period, is generally characterized as being heavily deformed and containing bubbles at the interfaces of the different ages of ice (Bjerkelund et al., 1985). The Lake Hazen ice cover of winter 2021/2022 likely experienced significant decay and deformation during summer 2022 before freezing temperatures resolidified and reconsolidated the ice, forming the MY ice. Any additions of snow at the surface would likely incorporate as snow-ice layers with possible bubble inclusions at their interfaces. At C-band wavelengths, increasing the RMS height deviation of internal interface bubbles from 0 to c. 5 mm can increase backscatter intensities from c. –22 to –7 dB (Murfitt et al., 2022). Although the structural composition of the Lake Hazen MY ice is not known, it is likely that heavily deformed MY ice with internal bubbled layers caused the large magnitude of difference in backscatter intensity between FY and the MY ice in winter 2022-2023.

3. Special backscatter features over Lake Untersee and Lake Obersee

3.1. Spatio-temporal variations of backscatter over Lake Obersee

The journal manuscript described the spatio-temporal patterns of backscatter intensity changes over Lake Untersee as radial, with switching generally commencing and ending along the shorelines at the onset of winter and summer, respectively. Lake Obersee, on the other hand, displays markedly different patterns of change. Each year of the SAR record at the change from low to high intensities in April, a spiral pattern of increasing intensities manifests in front of the Vangengejma Glacier forming an annular feature in the center of the lake before the rest of the lake surface switches from having low to high intensities (**Fig. 14**). In late-November, intensities over the whole lake switch rapidly from high to low intensities with the exception of a circular area in front of the Vangengejma Glacier (**Fig. 15**), the same area were the annular feature forms in April. The circular pattern was less visible in 2021 due to snow drifts over the lake surface following snow events that occurred around this time.

Consistent with the strong positive correlation found between ice thickness and the timing of backscatter intensity increase discussed in Chapter 2 (**Fig. 11**), the spiral/annular patterns that manifest over Lake Obersee suggest the ice cover is thinned in a similar way. In fact, a ground penetrating radar (GPR) transect across the Lake Obersee ice cover (**Fig. 16**) indicate the ice cover is thinner by between 4.3 and 8.9 % (around 400 and 1200 m along the GPR line, respectively) compared to the center of the lake (around 700 m) (**Fig. A3.3**), and these areas of thinning align with the spiral/annular backscatter feature in the SAR imagery. Over the Lake Untersee ice cover, variations in ice thickness are caused primarily by accelerated sublimation in regions with strong persistent winds (Faucher et al., 2019). Although patterns of sublimation are not known for the Lake Obersee ice cover, it is unlikely that accelerated sublimation occurs in such an annular pattern and for only the central region of Lake Obersee. Thus, the thinning that is observed in the GPR transect is likely the result of sub-aqueous thinning. Irrespective of the thinning process, the combined effects of rapid cooling and lower hydrostatic pressures under thinner ice would allow for earlier bubble nucleation at the onset of winter freezing compared to thicker regions.

The lack of correlation found between the timing of backscatter intensity decrease at the onset of summer over Lake Untersee is again reiterated for Lake Obersee; the relatively thicker central region of the ice cover observed in the GPR transect aligns with the high SAR backscatter intensities observed over the central region of the ice cover in late-November/early-December (**Fig. 15**). For Lake Untersee, it was suggested that the timing of backscatter intensity decrease could relate more to the monthly timescale lag of water column mixing (Steel et al., 2015) given this occurs independently of ice thickness. For Lake Obersee, the high intensity circular feature may similarly relate to a lag in water column mixing regimes; the central circular feature may relate to a stagnation of bubble-supporting waters where circulation velocities are lowest prior to full redistribution.

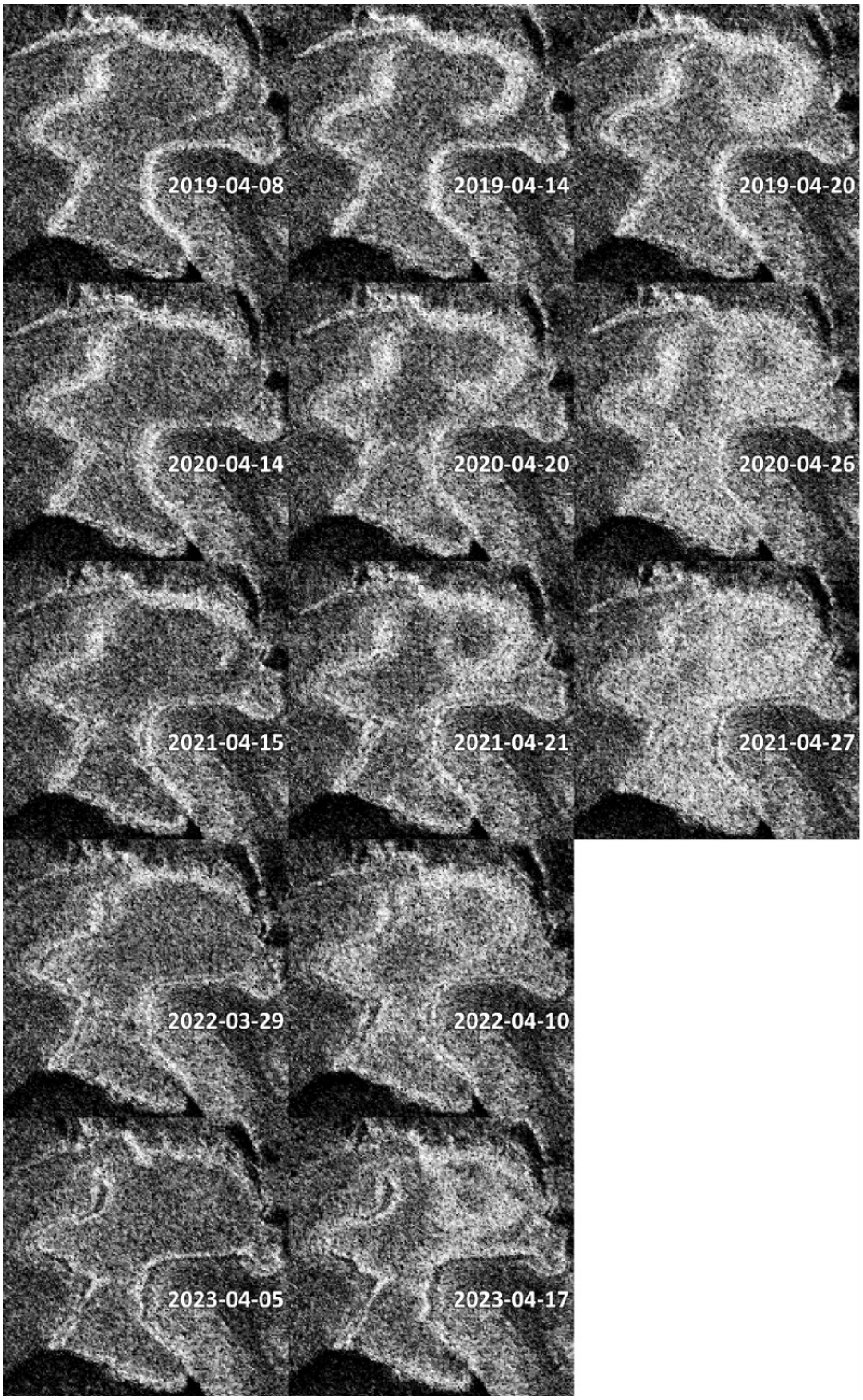

Fig. 14 Summer to winter backscatter patterns over Lake Obersee. The spatio-temporal patterns of SAR backscatter intensity (dB) change regularly observed over Lake Obersee between April and May during the 4 years of available SAR imagery (ascending trajectory). The images show reoccurring swirl/annular patterns each year at the change from low to high intensities.

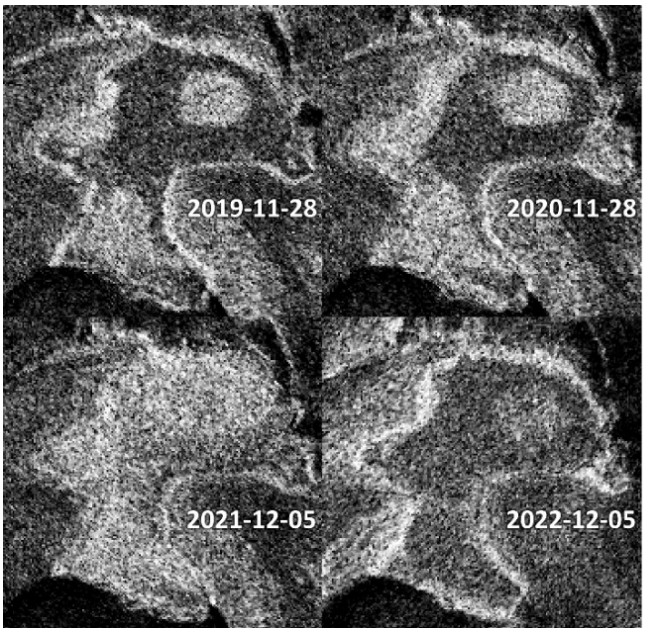

Fig. 15 Winter to summer backscatter patterns over Lake Obersee. The spatio-temporal patterns of SAR backscatter intensity (dB) change regularly observed over Lake Obersee in November during the 4 years of available SAR imagery. The images show a reoccurring circular pattern each year at the change from high to low intensities.

3.2. Impact of a GLOF on SAR backscatter over Lake Untersee and Lake Obersee

In January 2018, a glacial lake outburst flood (GLOF) originating from Lake Obersee drained down a channel between the Anuchin Glacier and the east lateral moraine into Lake Untersee. Due to the size difference between the two lakes, substantial impacts to the Lake Obersee ice cover were observed while the Lake Untersee ice cover was less affected.

The 2018/2019 GLOF drained c. 2.29×10^7 m^3 of water from Lake Obersee, causing the Lake Obersee ice cover to drop in elevation by c. 11 m during this period (Faucher et al., 2021). The ice cover grounded and became elevated above the new water level in regions where the water depth was 11 m or less. In the years following the initial event, the grounded ice cracked, buckled, and hollowed at its base as heat radiated from the sediments below, likely giving multiple bounces and volume scattering, resulting in high backscatter intensities along the shorelines (**Fig. 14**). Because the grounded ice was not replenished at its base and continually sublimated at the surface, the grounded ice progressively thinned over the course of several year to reveal the new shoreline, appearing as the widening dark features along the perimeter of the lake between 2021 and 2023.

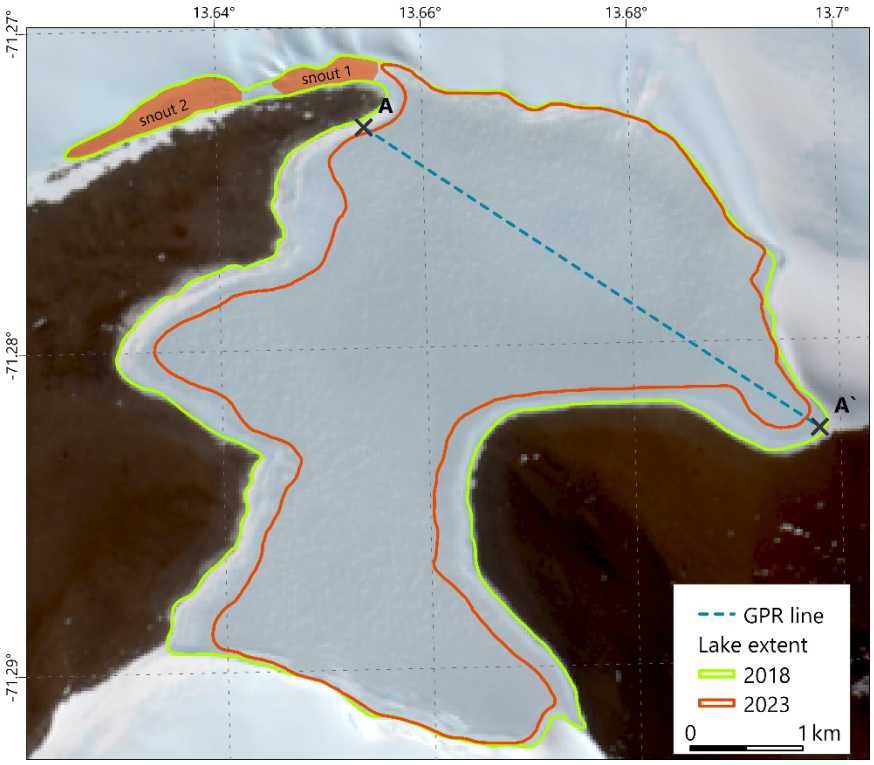

Fig. 16 Lake Obersee, Dronning Maud Land, East Antarctica. Location map showing the 2018 and 2023 ice cover extents (green and orange lines, respectively) and a GPR line across the ice cover (blue line). Background is Sentinel-2 MSI acquired on 12 January 2018, courtesy of ESA. Map generated using ArcGIS Pro.

The GLOF is believed to have originated from a small sub-basin extension of Lake Obersee located between the Vangengejma Glacier and a lateral moraine in the north-west of the lake (labeled "snout" in **Fig. 16**). This small sub-basin increased in volume over many years, after which a glacial shift in 2018 likely caused the breaching of a subaqueous retaining sill (Faucher et al., 2021), subsequently draining water from the sub-basin and lake until their levels were below the sill. Although the SAR record over the oasis begins after the initial GLOF, SAR intensity time series over the snout (**Fig. 17**) suggests water continued to drain from this area for several years following the initial event. The time series for the two snout areas show dips of intensities each year in December/January during the warm period. This suggests water was indeed still present below the ice cover in this area, and the presence/absence of bubbles and their abundance have seasonal responses like the rest of the lake. Additionally, the declining trends of intensities, as well as the shortening duration of the summer dips over time, indicate there is progressively less water below the ice cover in this area.

Fig. 17 Time series of SAR backscatter over Lake Obersee. Time series of SAR backscatter (dB) over Lake Obersee between February 2019 and June 2023 for the 2023 lake extent and western snout where the GLOF originated for **a)** ascending acquisitions and **b)** descending acquisitions.

The Lake Untersee ice cover experienced relatively few effects following the GLOF. Due to the difference in basin volume between the two lakes, the Lake Untersee water level increased by only c. 2 m. A temporary moat of several meters formed along the perimeter of parts of the lake. Although clearly visible in high resolution optical imagery, neither the moat nor the north-eastern melt-out hole from the influx of channel water can be clearly resolved in the SAR imagery (**Fig. A3.4**). This is likely because the first SAR image was acquired approximately 1 month after the initial GLOF, allowing surface water to freeze over. Furthermore, the resolution of Sentinel-1 imagery (c. 14 m^2) is too coarse to distinguish between the ice cover, the shoreline, and a narrow band of low backscatter caused by open specular moat water along the perimeter of the lake.

Slight decreasing and subsequent increasing trends were recorded in the Lake Untersee time series during the 2019 and 2020 winter periods, respectively, while intensities over Lake Obersee were relatively constant during the same periods (**Fig. 13**). These trends can be attributed to the reaction of water column dissolved gases following the GLOF event. Firstly, following the GLOF, a temporary moat formed along the perimeter of the lake which may have allowed for some degassing. Secondly, the in-pouring of GLOF water may have induced circulation in the Lake Untersee basin, causing gases to redistribute more rapidly than usual. Lastly, although Lake Obersee and Lake Untersee are similarly supersaturated in dissolved gases, supersaturated water flowing from Lake Obersee down the GLOF channel would degas and equilibrate with the atmosphere, having a diluting effect. Together, these processes may have resulted in a slight lowering of the dissolved gas concentrations in the Lake Untersee water column, ultimately affecting the abundance of bubbles below the ice cover. In fact, water column profiles from 2019 recorded relatively low saturations of DO compared to other years (**Fig. A3.5**). The subsequent increasing trend in winter 2020 likely reflects dissolved gases returning to normal conditions. No expeditions to Lake Untersee took place in 2020, so the rebound of DO is not corroborated.

Chapter 4: Concluding remarks

Backscatter variations over SIC lakes have been studied for over 50 years, helping monitor and better understand regional climate impacts. However, the seasonal backscatter response of PIC lakes in Antarctica lacks such documentation. This thesis and journal manuscript shows that Lake Untersee and other similar lakes in Antarctica have seasonal backscatter regimes resembling those observed over SIC Arctic lakes. The observations made in this thesis were unexplained and have challenged existing hypotheses on Arctic lake ice backscatter mechanisms. This work aimed to describe the seasonal backscatter regimes of PIC lakes and to explore possible explanations for their occurrence.

This study, using a dense stack of Sentinel-1 C-band SAR imagery over Lake Untersee in East Antarctica, reveals seasonal backscatter oscillations that are linked to air temperature. Video footage under the ice cover shows an abundance of radiometrically rough bubbles at the ice/water interface. The timing of backscatter intensity increase is strongly correlated with lake ice thickness variations. Together, this indicates that ice thickness controls the freezing period, the abundance of dissolved gas below the ice cover, and ultimately, the timing of bubble nucleation and abundance change. These results indicate that substantial and abrupt changes to backscatter intensity can occur independently of lake ice grounding and are driven primarily by the seasonal regimes of dissolved gas abundance in the water column.

This research has contributed to the scientific community on several fronts, including a first documentation of seasonal SAR backscatter regimes of PIC lakes in Antarctica, broadening the scope and general understanding of lake ice backscatter mechanisms, and providing significant evidence for the dominant contribution of dissolved gas abundance in certain lacustrine settings. Previously, the dynamics of dissolved gases and bubbles were only briefly considered in studies on Arctic lake ice backscatter. This thesis confirms and shows that these dynamic properties can have significant impacts on backscatter. As such, a characterization of the seasonal dynamics of dissolved gases and bubbles at the ice/water interface of PIC and SIC lakes and their effects on backscatter intensities is warranted in future studies. Doing so may have significant implications to the retrieval of interferometric information derived over lake ice, possibly providing a means to directly observe lake ice thickness from spaceborne SAR platforms.

References

Adams, E. E., Priscu, J. C., Fritsen, C. H., Smith, S. R., & Brackman, S. L. (1998). Permanent Ice Covers of the McMurdo Dry Valley Lakes, Antarctica: Bubble Formation and Metamorphism. In *Ecosystem Dynamics in a Polar Desert: the Mcmurdo Dry Valleys, Antarctica* (Vol. 72, pp. 281–295). https://doi.org/10.1029/ar072p0281

Andersen, D. T., McKay, C. P., & Lagun, V. (2015). Climate Conditions at Perennially Ice-Covered Lake Untersee, East Antarctica. *Journal of Applied Meteorology and Climatology*, *54*(7), 1393–1412. https://doi.org/10.1175/JAMC-D-14-0251.1

Andersen, D. T., McKay, C. P., & Wharton, R. A. (1998). Dissolved gases in perennially ice-covered lakes of the McMurdo Dry Valleys, Antarctica. *Antarctic Science*, *0*(2), 124–133.

Andersen, D. T., Sumner, D. Y., Hawes, I., Webster-Brown, J., & McKay, C. P. (2011). Discovery of large conical stromatolites in Lake Untersee, Antarctica. *Geobiology*, *9*(3), 280–293. https://doi.org/10.1111/j.1472-4669.2011.00279.x

Antonova, S., Duguay, C. R., Kääb, A., Heim, B., Langer, M., Westermann, S., & Boike, J. (2016). Monitoring Bedfast Ice and Ice Phenology in Lakes of the Lena River Delta Using TerraSAR-X Backscatter and Coherence Time Series. *Remote Sensing*, *8*(11). https://doi.org/10.3390/rs8110903

Atwood, D. K., Gunn, G. E., Roussi, C., Wu, J., Duguay, C., & Sarabandi, K. (2015). Microwave Backscatter from Arctic Lake Ice and Polarimetric Implications. *IEEE Transactions on Geoscience and Remote Sensing*, *53*(11), 5972–5982. https://doi.org/10.1109/TGRS.2015.2429917

Bjerkelund, C. A., Lapp, D. J., Ramseier, R. O., & Sinha, N. K. (1985). The Texture and fabric of the second year sea ice cover at Mould Bay, Prince Patrick Island, NWT, April 1983. *1985 IEEE International Geoscience and Remote Sensing Symposium, IGARSS*, *1*, 426–431.

Bryan, M. L., & Larson, R. W. (1973). *Application of dielectric constant measurements to radar imagery*.

Bryan, M. L., & Larson, R. W. (1975). The Study of Fresh-Water Lake Ice Using Multiplexed Imaging Radar. *Journal of Glaciology*, *14*(72), 445–457. https://doi.org/10.3189/s002214300002195x

Carte, A. E. (1961). Air Bubbles in Ice. *Proceedings of the Physical Society*, *77*, 757–768.

Castendyk, D. N., Obryk, M. K., Leidman, S. Z., Gooseff, M., & Hawes, I. (2016). Lake Vanda: A sentinel for climate change in the McMurdo Sound Region of Antarctica. *Global and Planetary Change*, *144*, 213–227. https://doi.org/10.1016/j.gloplacha.2016.06.007

Craig, H., Wharton, R. A., & McKay, C. P. (1992). Oxygen Supersaturation in Ice-Covered Antarctic Lakes: Biological Versus Physical Contributions. *Science*, *255*(5042), 318–321.

Doran, P. T., McKay, C. P., Fountain, A. G., Nylen, T., McKnight, D. M., Jaros, C., & Barrett, J. E. (2008). Hydrologic response to extreme warm and cold summers in the McMurdo Dry Valleys, East Antarctica. *Antarctic Science*, *20*(5), 499–509. https://doi.org/10.1017/S0954102008001272

Doran, P. T., Priscu, J. C., Lyons, W. B., Powell, R. D., Andersen, D. T., & Poreda, R. J. (2007). Paleolimnology of Extreme Cold Terrestrial and Extraterrestrial Environments. In R. Pienitz, M. S. v. Douglas, & J. P. Smol (Eds.), *Long-term Environmental Change in Arctic and Antarctic Lakes* (Vol. 8, p. 578). Springer.

Duguay, C. R., Pultz, T. J., Lafleur, P. M., & Drai, D. (2002). RADARSAT backscatter characteristics of ice growing on shallow sub-Arctic lakes, Churchill, Manitoba, Canada. *Hydrological Processes*, *16*(8), 1631–1644. https://doi.org/10.1002/hyp.1026

Elachi, C., Bryan, M. L., & Weeks, W. F. (1976). Imaging Radar Observations of Frozen Arctic Lakes. *REMOTE SENSING OF ENVIRONMENT*, *5*, 169–175.

Engram, M., Anthony, K. W., Meyer, F. J., & Grosse, G. (2012). Synthetic aperture radar (SAR) backscatter response from methane ebullition bubbles trapped by thermokarst lake ice. *Canadian Journal of Remote Sensing*, *38*(6), 667–682. http://pubs.casi.ca/journal/cjrs

Engram, M., Anthony, K. W., Meyer, F. J., & Grosse, G. (2013a). Characterization of L-band synthetic aperture radar (SAR) backscatter from floating and grounded lake ice in arctic Alaska. *The Cryosphere Discussions*, *7*, 2061–2088. https://doi.org/10.5194/tcd-7-2061-2013

Engram, M., Anthony, K. W., Meyer, F. J., & Grosse, G. (2013b). Characterization of L-band synthetic aperture radar (SAR) backscatter from floating and grounded thermokarst lake ice in Arctic Alaska. *Cryosphere*, *7*(6), 1741–1752. https://doi.org/10.5194/tc-7-1741-2013

Engram, M., Arp, C. D., Jones, B. M., Ajadi, O. A., & Meyer, F. J. (2018). Analyzing floating and bedfast lake ice regimes across Arctic Alaska using 25 years of space-borne SAR imagery. *Remote Sensing of Environment*, *209*, 660–676. https://doi.org/10.1016/j.rse.2018.02.022

Environment and Climate Change Canada. (2023, July 14). *Temperature and Precipitation Graph for 1981 to 2010 Canadian - Climate Normals: ALERT*.

Faucher, B., Lacelle, D., Fisher, D. A., Andersen, D. T., & McKay, C. P. (2019). Energy and water mass balance of Lake Untersee and its perennial ice cover, East Antarctica. *Antarctic Science*, *31*(5), 271–285. https://doi.org/10.1017/S0954102019000270

Faucher, B., Lacelle, D., Marsh, N. B., Jasperse, L., Clark, I. D., & Andersen, D. T. (2021). Glacial lake outburst floods enhance benthic microbial productivity in perennially ice-covered Lake Untersee (East Antarctica). *Communications Earth & Environment*, *2*(211), 1–12. https://doi.org/10.1038/s43247-021-00280-x

Freeman, A., & Durden, S. L. (1998). A Three-Component Scattering Model for Polarimetric SAR Data. *IEEE Transactions on Geoscience and Remote Sensing*, *36*(3), 963–973. https://doi.org/10.1109/36.673687

Gherboudj, I., Bernier, M., & Leconte, R. (2010). A Backscatter Modeling for River Ice: Analysis and Numerical Results. *IEEE Transactions on Geoscience and Remote Sensing*, *48*(4), 1788–1798. https://doi.org/10.1109/TGRS.2009.2034256

Groh, A., Ewert, H., Rosenau, R., Fagiolini, E., Gruber, C., Floricioiu, D., Jaber, W. A., Linow, S., Flechtner, F., Eineder, M., Dierking, W., & Dietrich, R. (2014). Mass, Volume and Velocity of the Antarctic Ice Sheet: Present-Day Changes and Error Effects. *Surveys in Geophysics*, *35*(6), 1481–1505. https://doi.org/10.1007/s10712-014-9286-y

Gunn, G. E., Duguay, C. R., Atwood, D. K., King, J., & Toose, P. (2018). Observing Scattering Mechanisms of Bubbled Freshwater Lake Ice Using Polarimetric RADARSAT-2 (C-Band) and UW-Scat (X- A nd Ku-Bands). *IEEE Transactions on Geoscience and Remote Sensing*, *56*(5), 2887–2903. https://doi.org/10.1109/TGRS.2017.2786158

Hermichen, W.-D., Kowski, P., & Wand, U. (1985). Lake Untersee, a first isotope study of the largest freshwater lake in the interior of East Antarctica. *Nature*, *315*, 131–133.

Hoffman, M. J., Fountain, A. G., & Liston, G. E. (2008). Surface energy balance and melt thresholds over 11 years at Taylor Glacier, Antarctica. *Journal of Geophysical Research: Earth Surface*, *113*(4), 1–12. https://doi.org/10.1029/2008JF001029

Hood, E. M., Howes, B. L., & Jenkins, W. J. (1998). Dissolved gas dynamics in perennially ice-covered Lake Fryxell, Antarctica. *Limnology and Oceanography*, *43*(2), 265–272. https://doi.org/10.4319/lo.1998.43.2.0265

Jeffries, M. O., Morris, K., Weeks, W. F., & Wakabayashi, H. (1994). Structural and stratigraphic features and ERS 1 synthetic aperture radar backscatter characteristics of ice growing on shallow lakes in NW Alaska, winter 1991-1992. *Journal of Geophysical Research*, *99*(C11), 22459–22471. https://doi.org/10.1029/94jc01479

Jeffries, M. O., Wakabayashi, H., & Weeks, W. F. (1993). ERS-1 SAR backscatter changes associated with ice growing on shallow lakes in arctic Alaska. *International Geoscience and Remote Sensing Symposium (IGARSS)*, *4*, 2001–2004. https://doi.org/10.1109/igarss.1993.322048

Köck, G., Muir, D., Yang, F., Wang, X., Talbot, C., Gantner, N., & Moser, D. (2012). Bathymetry and Sediment Geochemistry of Lake Hazen (Quttinirpaaq National Park, Ellesmere Island, Nunavut) BATHYMETRY AND SEDIMENT GEOCHEMISTRY OF LAKE HAZEN • 57. *ARCTIC*, *65*(1), 56–66.

Lawrence, M. J. F., & Hendy, C. H. (1985). Water column and sediment characteristics of lake fryxell, taylor valley, Antarctica. *New Zealand Journal of Geology and Geophysics*, *28*(3), 543–552. https://doi.org/10.1080/00288306.1985.10421206

Leconte, R., & Klassen, P. D. (1991). Lake and River Ice Investigations in Northern Manitoba Using Airborne SAR Imagery. *Arctic*, *44*(Supplement 1), 153–163.

Lehnherr, I., St Louis, V. L., Sharp, M., Gardner, A. S., Smol, J. P., Schiff, S. L., Muir, D. C. G., Mortimer, C. A., Michelutti, N., Tarnocai, C., St Pierre, K. A., Emmerton, C. A., Wiklund, J. A., Köck, G., Lamoureux, S. F., & Talbot, C. H. (2018). The world's largest High Arctic lake responds rapidly to climate warming. *Nature Communications*, *9*(1290). https://doi.org/10.1038/s41467-018-03685-z

Lipp, G., Körber, C. H., Englich, S., Hartmann, U., & Rau, G. (1987). Investigation of the Behavior of Dissolved Gases during Freezing. *CRYOBIOLOGY*, *24*, 489–503.

Mahmud, M. S., Nandan, V., Howell, S. E. L., Geldsetzer, T., & Yackel, J. (2020). Seasonal evolution of L-band SAR backscatter over landfast Arctic sea ice. *Remote Sensing of Environment*, *251*. https://doi.org/10.1016/j.rse.2020.112049

Marsh, N. B., Lacelle, D., Faucher, B., Cotroneo, S., Jasperse, L., Clark, I. D., & Andersen, D. T. (2020). Sources of solutes and carbon cycling in perennially ice-covered Lake Untersee, Antarctica. *Scientific Reports*, *10*(1), 1–12. https://doi.org/10.1038/s41598-020-69116-6

Matzler, C., & Wegmuller, U. (1987). Dielectric properties of freshwater ice at microwave frequencies. *Journal of Physics D: Apply Physics* , *20*, 1623–1630.

McKay, C. P., Clow, G. D., Andersen, D. T., & Wharton, R. A. (1994). Light transmission and reflection in perennially ice-covered Lake Hoare, Antarctica. *Journal of Geophysical Research*, *99*(C10), 20427–20444. https://doi.org/10.1029/94jc01414

McKay, C. P., Clow, G. D., Wharton Jr, R. A., & Squyres, S. W. (1985). Thickness of ice on perennially frozen lakes. *Nature*, *313*(14), 561–562.

Meissner, T., & Wentz, F. J. (2004). The complex dielectric constant of pure and sea water from microwave satellite observations. *IEEE Transactions on Geoscience and Remote Sensing*, *42*(9), 1836–1849. https://doi.org/10.1109/TGRS.2004.831888

Mellor, J. C. (1982). *Bathymetry of Alaskan Arctic Lakes: A Key to Resource Inventory with Remote-Sensing Methods*.

Morris, K., Jeffries, M. O., & Weeks, W. F. (1995). Ice processes and growth history on Arctic and sub-Arctic lakes using ERS-1 SAR data. *Polar Record*, *31*(177), 115–128.

Muguruma, J., & Kikuchi, K. (1963). Lake Ice Investigation at Peters Lake, Alaska. *Journal of Glaciology*, *4*(36), 689–708. https://doi.org/10.3189/s0022143000028318

Mullan, D., Swindles, G., Patterson, T., Galloway, J., Macumber, A., Falck, H., Crossley, L., Chen, J., & Pisaric, M. (2017). Climate change and the long-term viability of the World's busiest heavy haul ice road. *Theoretical and Applied Climatology*, *129*(3–4), 1089–1108. https://doi.org/10.1007/s00704-016-1830-x

Murfitt, J., Duguay, C., Picard, G., & Gunn, G. (2023). Forward modelling of synthetic aperture radar backscatter from lake ice over Canadian Subarctic Lakes. *Remote Sensing of Environment*, *286*. https://doi.org/10.1016/j.rse.2022.113424

Murfitt, J., & Duguay, C. R. (2020). Assessing the Performance of Methods for Monitoring Ice Phenology of the World's Largest High Arctic Lake Using High-Density Time Series Analysis of Sentinel-1 Data. *Remote Sensing*, *12*(382), 1–25. https://doi.org/10.3390/rs12030382

Murfitt, J., & Duguay, C. R. (2021). 50 years of lake ice research from active microwave remote sensing: Progress and prospects. *Remote Sensing of Environment*, *264*, 1–21. https://doi.org/10.1016/j.rse.2021.112616

Murfitt, J., Duguay, C. R., Picard, G., & Gunn, G. E. (2022). Investigating the Effect of Lake Ice Properties on Multifrequency Backscatter Using the Snow Microwave Radiative Transfer Model. *IEEE Transactions on Geoscience and Remote Sensing*, *60*. https://doi.org/10.1109/TGRS.2022.3197109

Obryk, M. K., Doran, P. T., Fountain, A. G., Myers, M., & McKay, C. P. (2020). Climate From the McMurdo Dry Valleys, Antarctica, 1986–2017: Surface Air Temperature Trends and Redefined Summer Season. *Journal of Geophysical Research: Atmospheres*, *125*(13). https://doi.org/10.1029/2019JD032180

Obryk, M. K., Doran, P. T., & Priscu, J. C. (2014). The permanent ice cover of Lake Bonney, Antarctica: The influence of thickness and sediment distribution on photosynthetically available radiation and chlorophyll-a distribution in the underlying water column. *Journal of Geophysical Research: Biogeosciences*, *119*(9), 1879–1891. https://doi.org/10.1002/2014jg002672

Parker, B. C., Simmons, G. M., Seaburg, K. G., Cathey, D. D., & Allnutt, F. C. T. (1982). Comparative ecology of plankton communities in seven Antarctic oasis lakes. *Journal of Plankton Research*, *4*(2), 271–286. https://academic.oup.com/plankt/article/4/2/271/1466087

Priscu, J. C., Fritsen, C. H., Adams, E. E., Giovannoni, S. J., Paerl, H. W., & McKay, C. P. (1998). Perennial Antarctic lake ice: an oasis for life in a polar desert. *Science*, *280*(5372), 5372.

Rignot, E., Echelmeyer, K., & Krabill, W. (2001). Penetration depth of interferometric synthetic-aperture radar signals in snow and ice. *Geophysical Research Letters*, *28*(18), 3501–3504. https://doi.org/10.1029/2000GL012484

Rouse, W. R., Oswald, C. J., Binyamin, J., Spence, C., Schertzer, W. M., Blanken, P. D., Bussières, N., & Duguay, C. R. (2005). The Role of Northern Lakes in a Regional Energy Balance. *Journal of Hydrometeorology*, *6*(3), 291–305.

Schutte, C. A., Samarkin, V. A., Peters, B., Madigan, M. T., Bowles, M., Morgan-Kiss, R., Casciotti, K., & Joye, S. (2020). Vertical stratification and stability of biogeochemical

processes in the deep saline waters of Lake Vanda, Antarctica. *Limnology and Oceanography*, *65*(3), 569–581. https://doi.org/10.1002/lno.11327
Schwab, M. J. (1998). Reconstruction of the late Quaternary climatic and environmental history of the Schirmacher Oasis and the Wohlthat Massif (East Antarctica). *Reports on Polar Research*, *293*, 1–128.
Sellmann, P. v, Weeks, W. F., & Campbell, W. J. (1975). Use of side-looking airborne radar to determine lake depth on the Alaskan North Slope. *Cold Regions Research and Engineering Laboratory*, *Special Report 230*.
St. Pierre, K. A., St. Louis, V. L., Lehnherr, I., Schiff, S. L., Muir, D. C. G., Poulain, A. J., Smol, J. P., Talbot, C., Ma, M., Findlay, D. L., Findlay, W. J., Arnott, S. E., & Gardner, A. S. (2019). Contemporary limnology of the rapidly changing glacierized watershed of the world's largest High Arctic lake. *Scientific Reports*, *9*(4447). https://doi.org/10.1038/s41598-019-39918-4
Steel, H. C. B., McKay, C. P., & Andersen, D. T. (2015). Modeling circulation and seasonal fluctuations in perennially ice-covered and ice-walled lake untersee, antarctica. *Limnology and Oceanography*, *60*(4), 1139–1155. https://doi.org/10.1002/lno.10086
Stiles, W. H., & Ulaby, F. T. (1980). The active and passive microwave response to snow parameters. 1. Wetness. *Journal of Geophysical Research*, *85*(C2), 1037–1044. https://doi.org/10.1029/JC085iC02p01037
Sumner, D. Y., Jungblut, A. D., Hawes, I., Andersen, D. T., Mackey, T. J., & Wall, K. (2016). Growth of elaborate microbial pinnacles in Lake Vanda, Antarctica. *Geobiology*, *14*(6), 556–574. https://doi.org/10.1111/gbi.12188
Surdu, C. M., Duguay, C. R., Pour, H. K., & Brown, L. C. (2015). Ice freeze-up and break-up detection of shallow lakes in Northern Alaska with spaceborne SAR. *Remote Sensing*, *7*(5), 6133–6159. https://doi.org/10.3390/rs70506133
Ulaby, F. T., & Long, D. G. (2014). *Microwave Radar and Radiometric Remote Sensing*. The University of Michigan Press.
Vincent, W., & Laybourn-Parry, J. (2008). *Polar Lakes and Rivers: Limnology of Arctic and Antarctic Aquatic Ecosystems*. Oxford University Press.
Wand, U., Samarkin, V. A., Nitzsche, H.-M., & Hubberten, H.-W. (2006). Biogeochemistry of methane in the permanently ice-covered Lake Untersee, central Dronning Maud Land, East Antarctica. *Limnol. Oceanogr*, *51*(2), 1180–1194.
Wand, U., Schwab, M., Samarkin, W., & Schachtschneider, D. (1996). Sedimentgeologische Arbeiten wahrend der Expedition Schirmacheroase 1994/95 des AWI, Forschungsstelle Potsdam in Arbeiten der AWI-Forschungsstelle Potsdam in Antarktika, 1994/95. *Ber Polarforsch*, *215*, 73–121.
Wand, U., Schwarz, G., Brüggemann, E., & Bräuer, K. (1997). Evidence for physical and chemical stratification in lake untersee (central Dronning Maud Land, East Antarctica). *Antarctic Science*, *9*(1), 43–45. https://doi.org/10.1017/s0954102097000060
Weber Hoen, E., & Zebker, H. A. (2000). Penetration depths inferred from interferometric volume decorrelation observed over the Greenland ice sheet. *IEEE Transactions on Geoscience and Remote Sensing*, *38*(6), 2571–2583. https://doi.org/10.1109/36.885204
Weeks, W. F., Fountain, A. G., Bryan, M. L., & Elachi, C. (1978). Differences in radar return from ice-covered North Slope Lakes. *Journal of Geophysical Research*, *83*(C8), 4069–4073. https://doi.org/10.1029/jc083ic08p04069

Wharton, R. A., McKay, C. P., Mancinelli, R. L., & Simmons, G. M. (1987). Perennial N2 supersaturation in an Antarctic lake. *Nature*, *325*, 343–345.

Yamaguchi, Y., Moriyama, T., Ishido, M., & Yamada, H. (2005). Four-Component Scattering Model for Polarimetric SAR Image Decomposition. *IEEE Transactions on Geoscience and Remote Sensing*, *43*(8), 1699–1706. https://doi.org/10.1109/TGRS.2005.852084

Yoshimura, K., Inada, T., & Koyama, S. (2008). Growth of spherical and cylindrical oxygen bubbles at an ice-water interface. *Crystal Growth and Design*, *8*(7), 2108–2115. https://doi.org/10.1021/cg070251k

Appendices

Appendix 1: Supplementary information to the journal manuscript

Supplementary Table 1 Water depth and ice thickness measurements from 14 borehole locations around the Lake Untersee ice cover acquired during the 2022 field expedition.

	Lat, long	Water depth, m	Ice thickness, cm
BH01	-71.33098, 13.45572	27	401
BH02	-71.33688, 13.47591	165	399
BH03	-71.35783, 13.42221	77	259
BH04	-71.35310, 13.44011	116	266
BH05	-71.34858, 13.45743	115	317
BH06	-71.34250, 13.48068	49	351
BH07	-71.33805, 13.49737	94	374
BH08	-71.33536, 13.50762	100	298
BH09	-71.32960, 13.53300	98	258
BH10	-71.34291, 13.50245	57	372
BH11	-71.33413, 13.46457	69	393
BH12	-71.34915, 13.42582	31	273
BH13	-71.34336, 13.42889	49	306
BH14	-71.33535, 13.52725	64	242

Supplementary Note 1: Effects of snow on Lake Untersee backscatter intensities

Lake Untersee experienced unusual patterns of elevated backscatter intensities between 23 November 2021 and 10 April 2022 as snow covered the surface and was later redistributed. Relatively large snowfalls of 2 and 5 cm occurred on 23 and 24 November, respectively, during the 2021 field expedition. Snow was observed to become quickly redistributed by the persistent southerly winds into the north of the lake over the course of several weeks. Because the snowfall events occurred at the same time as the expected intensity drop-offs that typically occur in late-November, the SAR imagery showed intensities decreasing in a south-east to north-west direction (**Supplementary Fig. 1**). The time series of 4 boreholes distributed linearly across the lake in this orientation (BH06, BH02, BH11, and BH01) show intensities are affected by snow between 23 November 2021 and 26 January 2022: BH06 (the site farthest south-east) is relatively unaffected and experiences a sudden drop-off in November/December 2021, while the three other sites do not experience a drop-off and intensities are generally higher and for a longer period of time at the sites that are farther north-west (**Supplementary Fig. 2**). Of the 4 sites,

BH11 was most affected by snow. The average intensity over this site in the weeks following the snow events (23 November 2021 to 4 January 2022) was –6.6 dB. This is similar to intensities recorded at this site during the previous high backscatter period (–6.4 dB between May and November 2021). In comparison, the average intensity at BH11 between 22 November 2020 to 3 January 2021 (the equivalent snow free period in the previous year) was –14.7 dB, more than 2-times lower than when snow fell on this this site in November 2021. This shows that snow cover over floating lake ice can produce backscatter intensities with values similar to the high backscatter period. However, optical satellite imagery acquired during the SAR record shows the ice cover to be largely free of snow between September and March (**Supplementary Note 2**). When snow is present at the surface, it is often only visible in the north and north-west sectors due to rapid redistribution by the persistent winds.

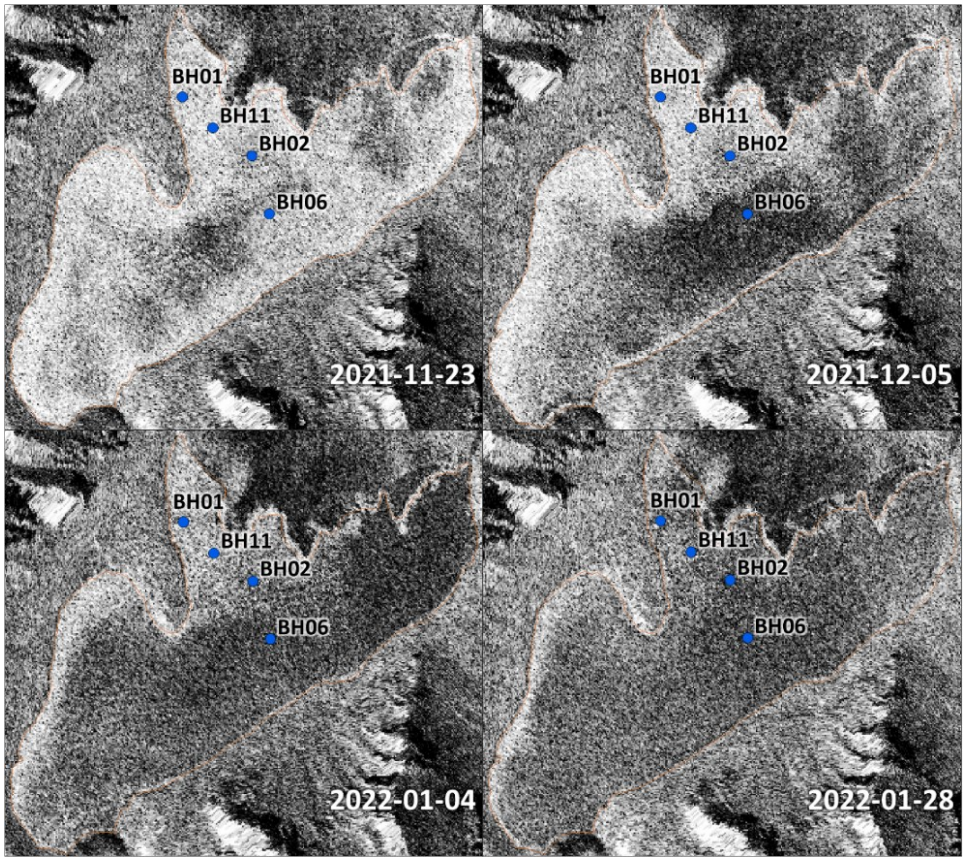

Supplementary Fig. 1 Effects of snow redistribution over Lake Untersee. SAR backscatter intensity (dB) over Lake Untersee following two snowfall events that occurred on 23 and 24 November 2021. High intensities over the lake are associated with the pattern of redistribution of snow into the north and north-west sectors of the lake.

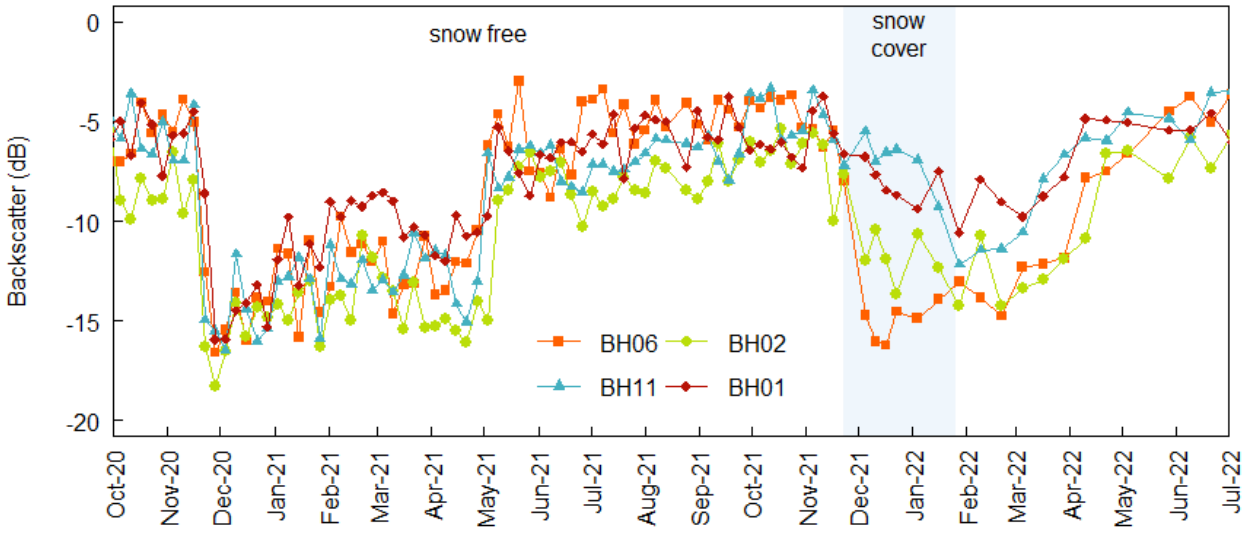

Supplementary Fig. 2 Effects of snow redistribution on time series. Time series of SAR backscatter (dB) in ascending trajectory over BH06, BH02, BH11, and BH01 between October 2020 and July 2022 to illustrate the effect of snow redistribution over Lake Untersee. The blue area indicates the period when snow was present at the surface of the lake.

Supplementary Note 2: Optical imagery over the Untersee Oasis

The following is a montage of available Sentinel-2 MSI images between October 2017 and March 2023. The imagery is courtesy of ESA and was accessed through Google Earth Engine. Optical imagery is only available during the period of solar illumination (between c. September and March). Little to no snow is visible on the lake ice surface each year between September and March.

2017-2018

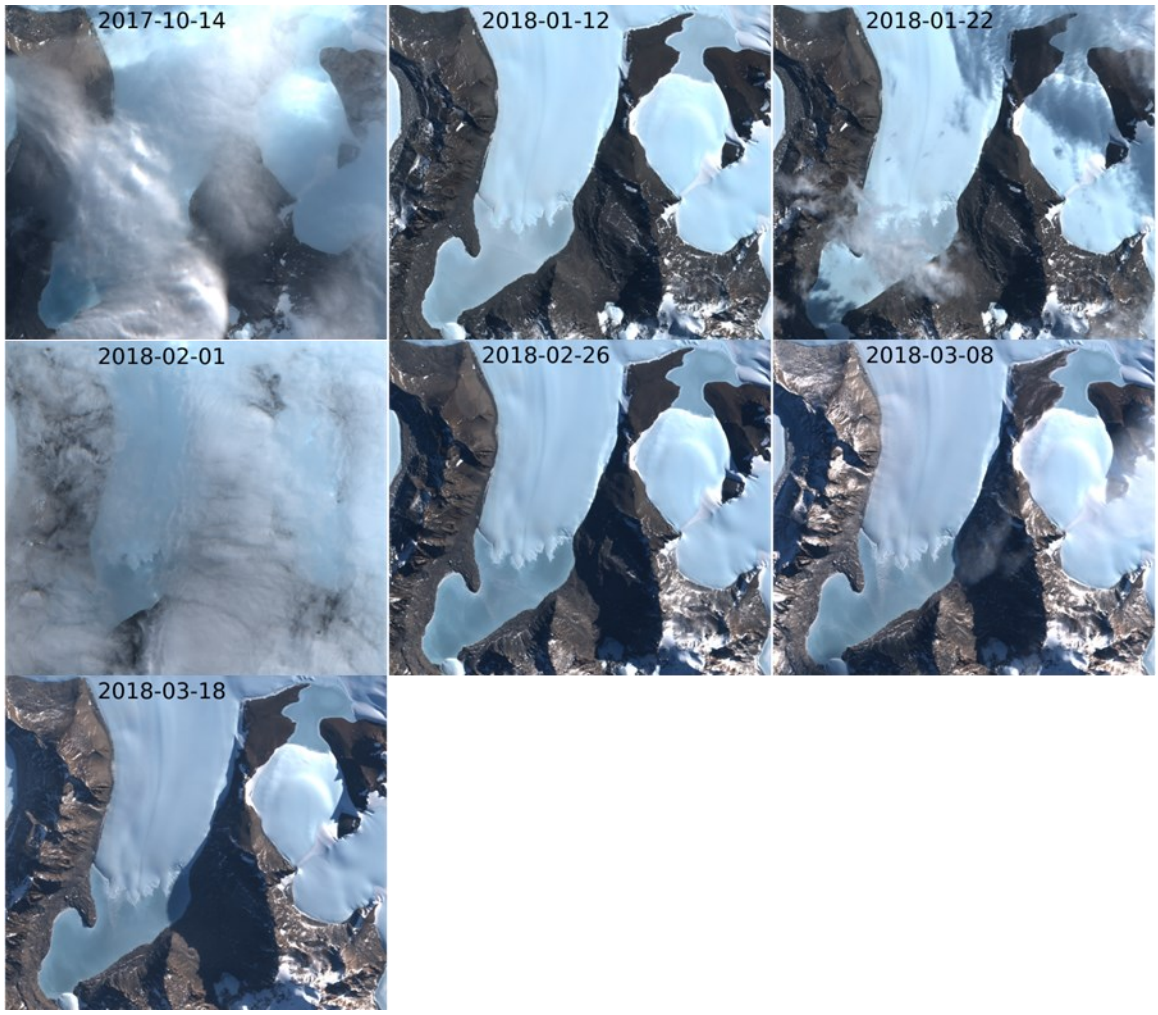
2017-10-14
2018-01-12
2018-01-22
2018-02-01
2018-02-26
2018-03-08
2018-03-18

2018-2019


2018-09-14
2018-09-24
2018-10-04
2018-10-14
2018-11-03
2018-11-23
2018-12-06
2018-12-13
2018-12-23
2019-01-02
2019-01-22
2019-02-01
2019-02-11
2019-03-03
2019-03-13

2019-2020


2019-09-09
2019-09-19
2019-09-29
2019-10-19
2019-11-08
2019-11-18
2019-11-28
2019-12-08
2019-12-28
2020-01-17
2020-01-27
2020-02-06
2020-02-16
2020-02-26
2020-03-17

2020-2021


2020-09-13
2020-09-23
2020-10-13
2020-11-02
2020-11-22
2020-12-02
2020-12-12
2020-12-22
2021-01-01
2021-01-21
2021-01-31
2021-02-10
2021-03-02
2021-03-12
2021-03-22

2021-2022

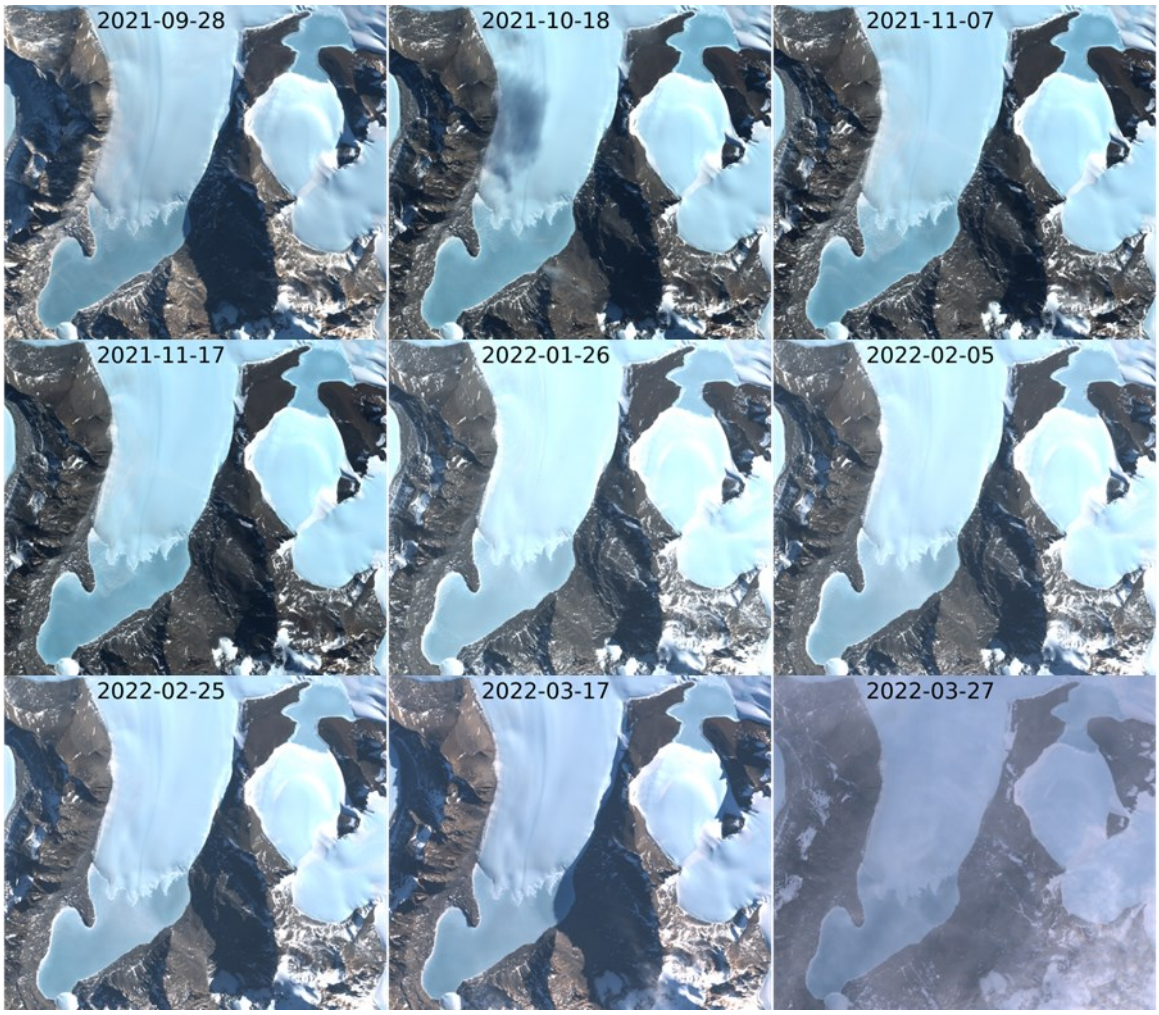
2021-09-28
2021-10-18
2021-11-07
2021-11-17
2022-01-26
2022-02-05
2022-02-25
2022-03-17
2022-03-27

2022-2023

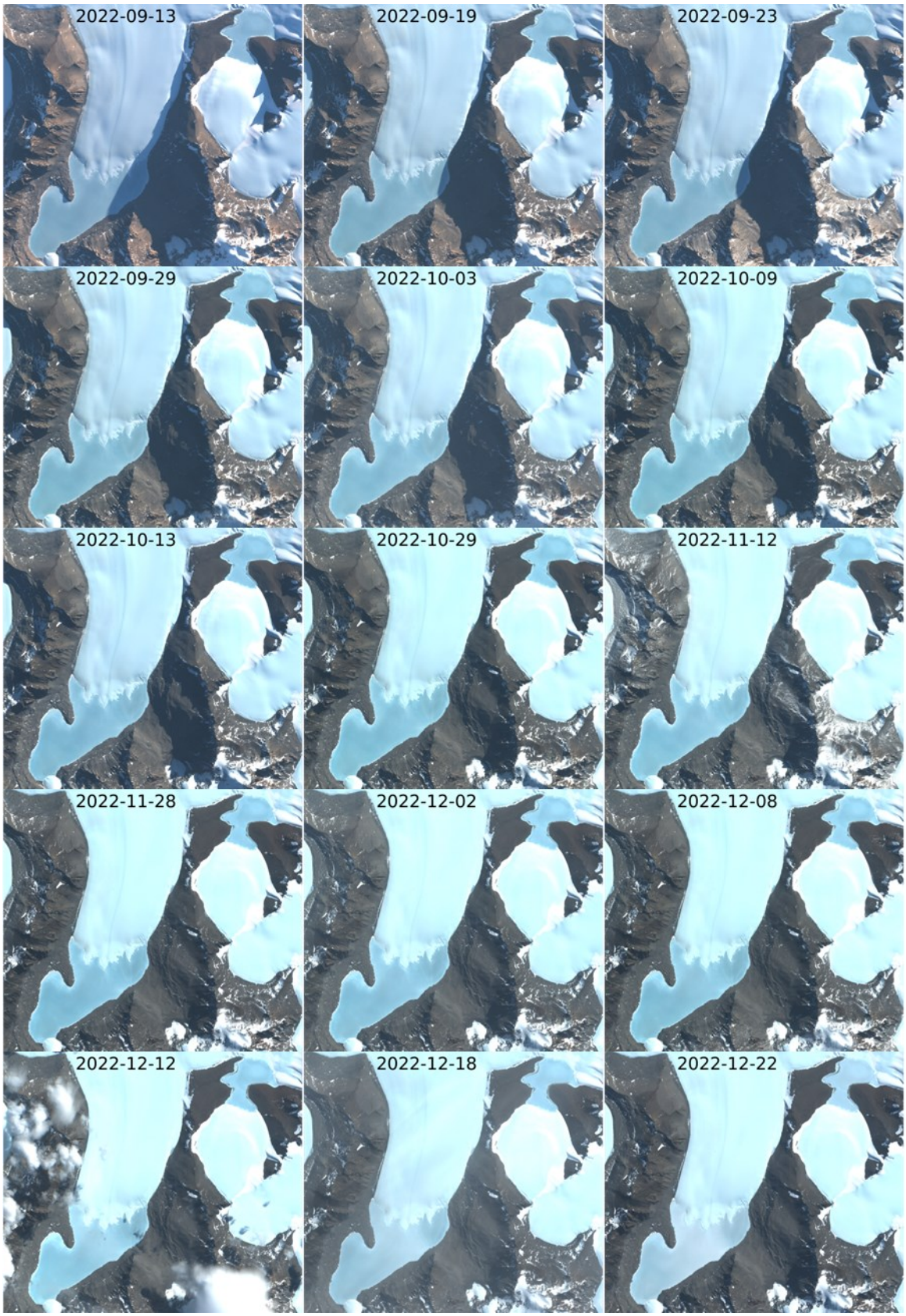
2022-09-13
2022-09-19
2022-09-23
2022-09-29
2022-10-03
2022-10-09
2022-10-13
2022-10-29
2022-11-12
2022-11-28
2022-12-02
2022-12-08
2022-12-12
2022-12-18
2022-12-22

2022-2023 (con't)

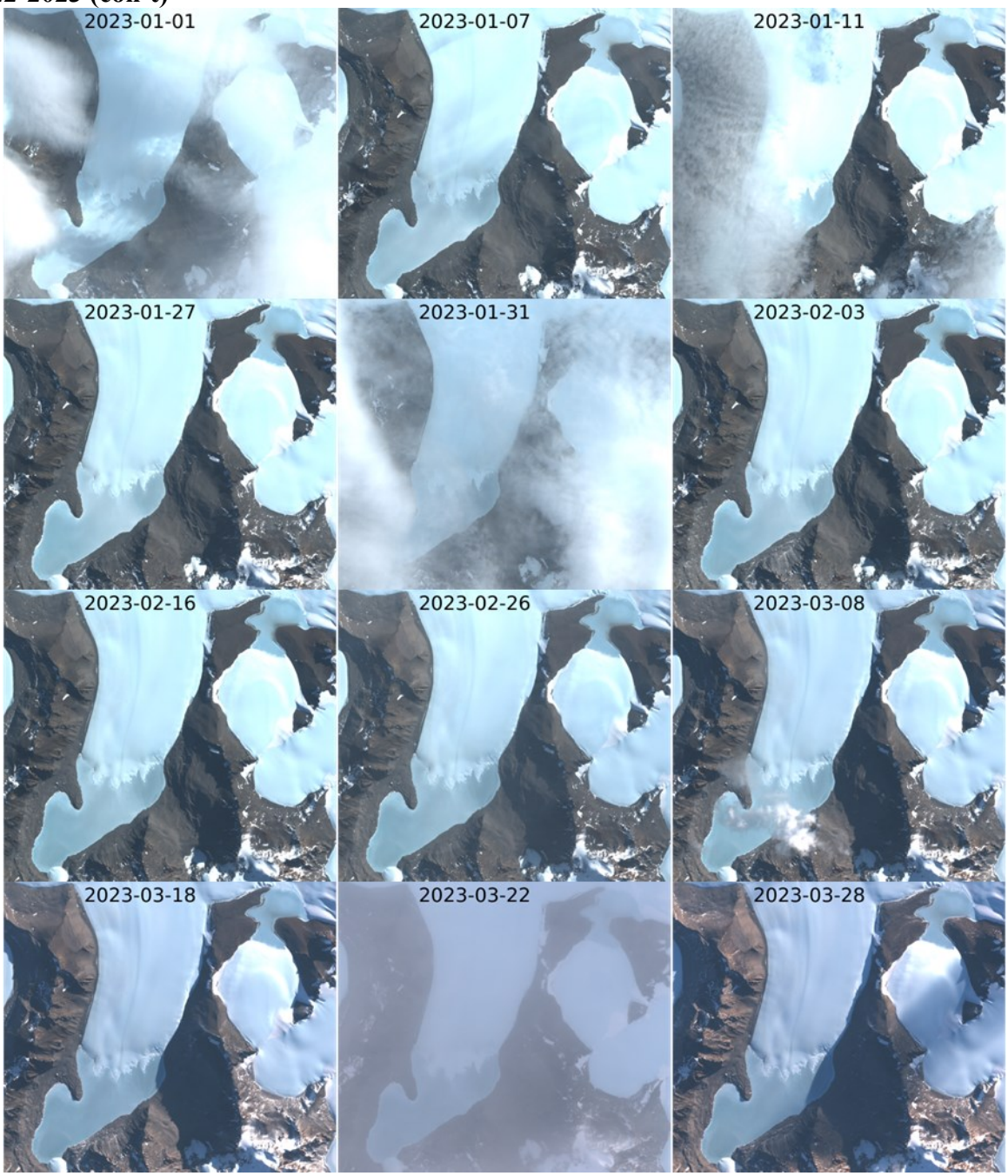

Supplementary Note 3: Supplementary ice covers

The seasonal backscatter frequency distribution of Lake Untersee and additional ice covers are presented to broaden the context of backscatter responses over floating ice covers. The additional ice covers include Lake Obersee, a second well-sealed PIC lake in the Untersee Oasis, Lake Vanda and Lake Fryxell, two moat-forming PIC lakes located in the McMurdo Dry Valleys in Antarctica, Lake Hazen, a SIC lake located in Nunavut on Ellesmere Island in the Canadian high Arctic, and sea ice in the vicinity of the Queen Elizabeth Islands (QEI) in the Canadian Arctic Archipelago. The methods used to acquire and process the imagery for the additional lake ice covers are the same as described in the Methods sections using the descending trajectory acquisitions of Sentinel-1 for the same period described for Lake Untersee. The frequency distributions for sea ice are from Mahmud et al. (2020) derived from RADARSAT-2 for the months November-December, January-May in 2009.

Appendix 2: Multi-year ice over Lake Hazen

Although full ice-off over Lake Hazen has become more common in recent times (Lehnherr et al., 2018), Sentinel-1 imagery over the lake shows that section 1 was completely covered by bright MY ice between October 2022 and June 2023 (**Fig. A2.1**). Murfitt & Duguay (2020) did not report any MY ice over Lake Hazen in their backscatter study utilizing Sentinel-1 imagery between November 2014 and February 2019. Therefore, 2023 marks the first year in almost a decade in which the water surface was not completely clear of ice. Thus, extending the full ice-off summary given in Lehnherr et al. (2018), 93 % of the period between November 2014 and June 2023 (the combined period from Murfitt & Duguay, 2020, and this study) has full ice-off for one month or more.

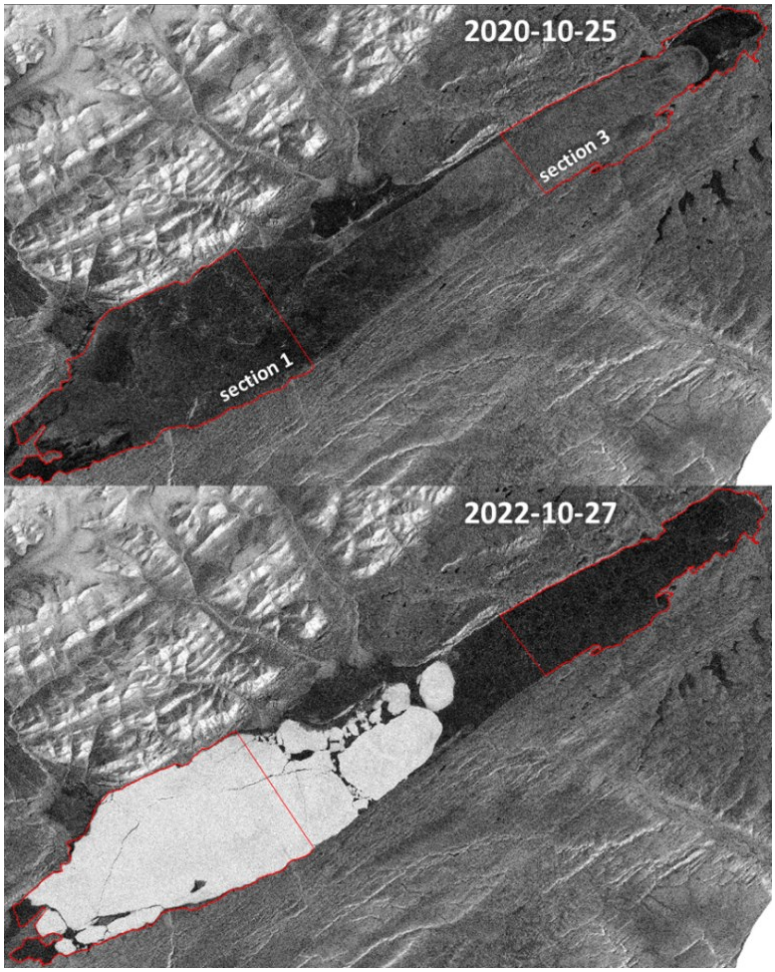

Fig. A2. 1 Multi-year ice over Lake Hazen. Multi-year ice at the surface of Lake Hazen between October 2022 and June 2023. Only first year ice has been observed at the surface during the same period since at least November 2014. Delineation of sections 1 and 3 are the same as in Murfitt & Duguay (2020).

Appendix 3: Supporting figures

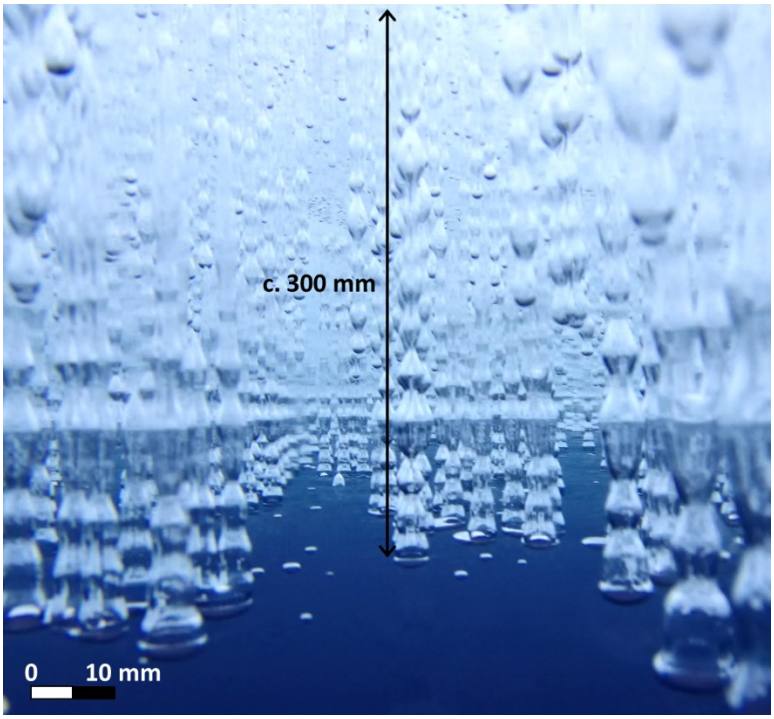

Fig. A3. 1 Bubbles inside the ice cover of Lake Untersee. Frame extracted from video footage captured while lowering the camera down the borehole at sites BH02 on 1 December 2022. Long tubular bubbles extend beyond the top of the image frame. Note, the scale bar is only accurate immediately in front of the camera. Photos taken by A. Gaudreau using a submersible video camera attached to a rope.

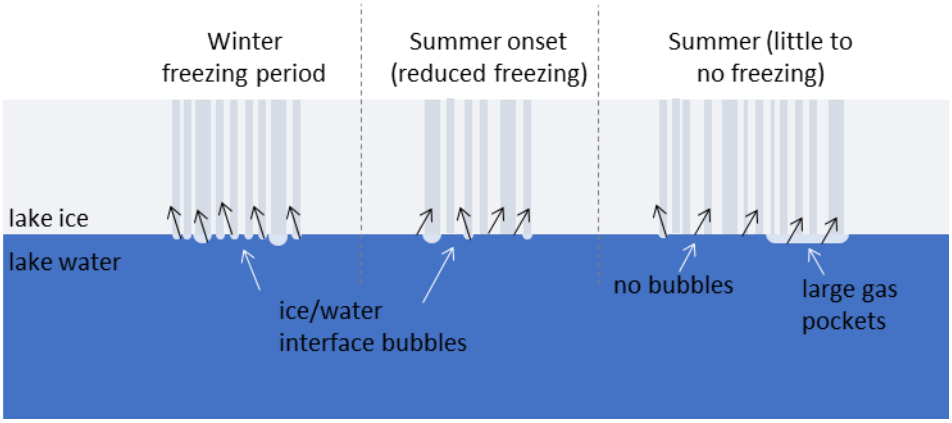

Fig. A3. 2 Evolution of bubbles at the ice/water interface. Bubble abundance at the ice/water interface decreases between the winter freezing period and the warm summer period with little freezing, leading to fewer scatterers and reduced backscatter intensity.

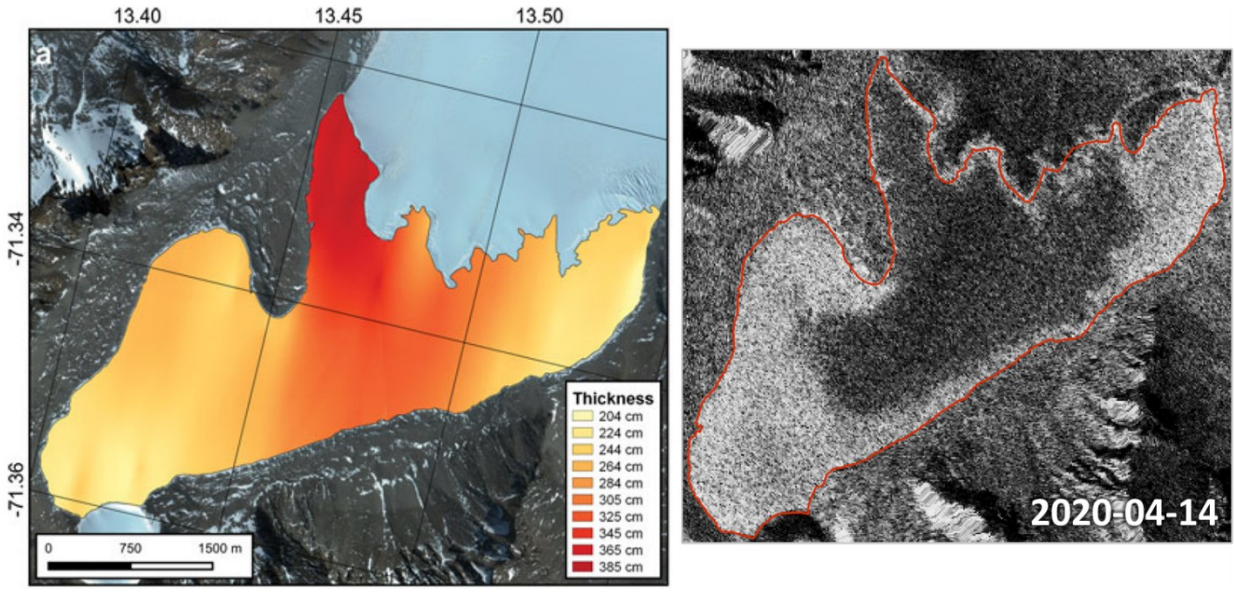

Fig. A3. 3. Spatial relationship of ice thickness and backscatter change. At the onset of winter, backscatter intensities over the ice cover (**right**) change from low to high in a patern similar to the gradients of ice thickness (**left**). Ice thickness map from Faucher et al. (2019).

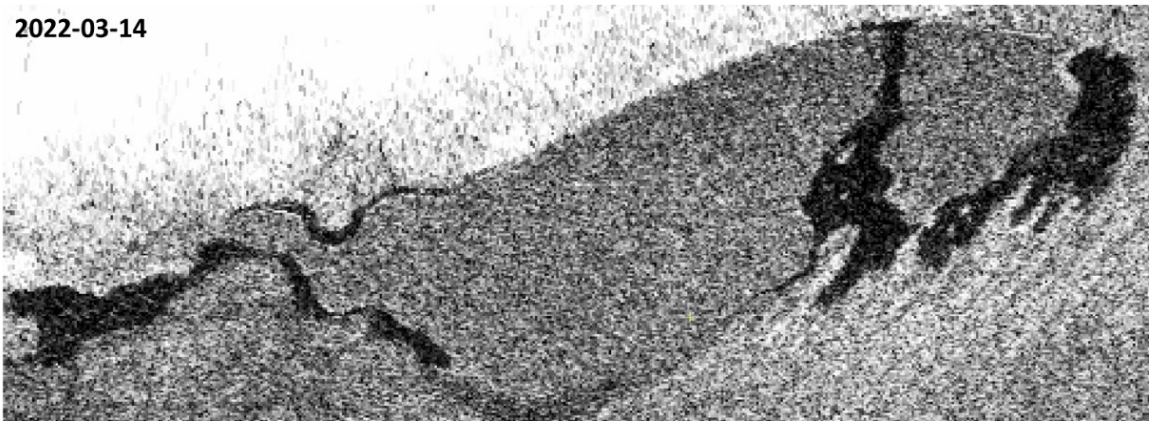

Fig. A3. 4 Backscatter over Lake Vanda. The Lake Vanda ice cover can experience significant decay in summer, causing large areas of (dark) open water to appear.

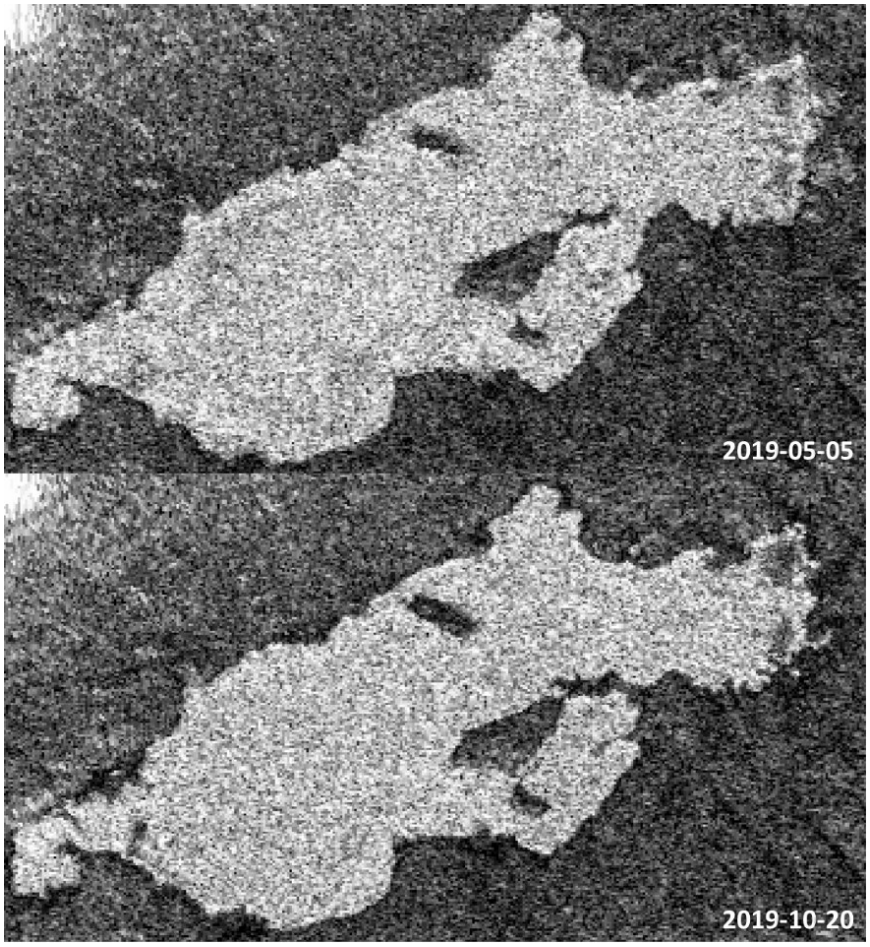

Fig. A3. 5 Backscatter over Lake Fryxell. Backscatter over Lake Fryxell between the beginning and end of winter shows that parts of the ice cover perimeter become darker, indicating grounding.

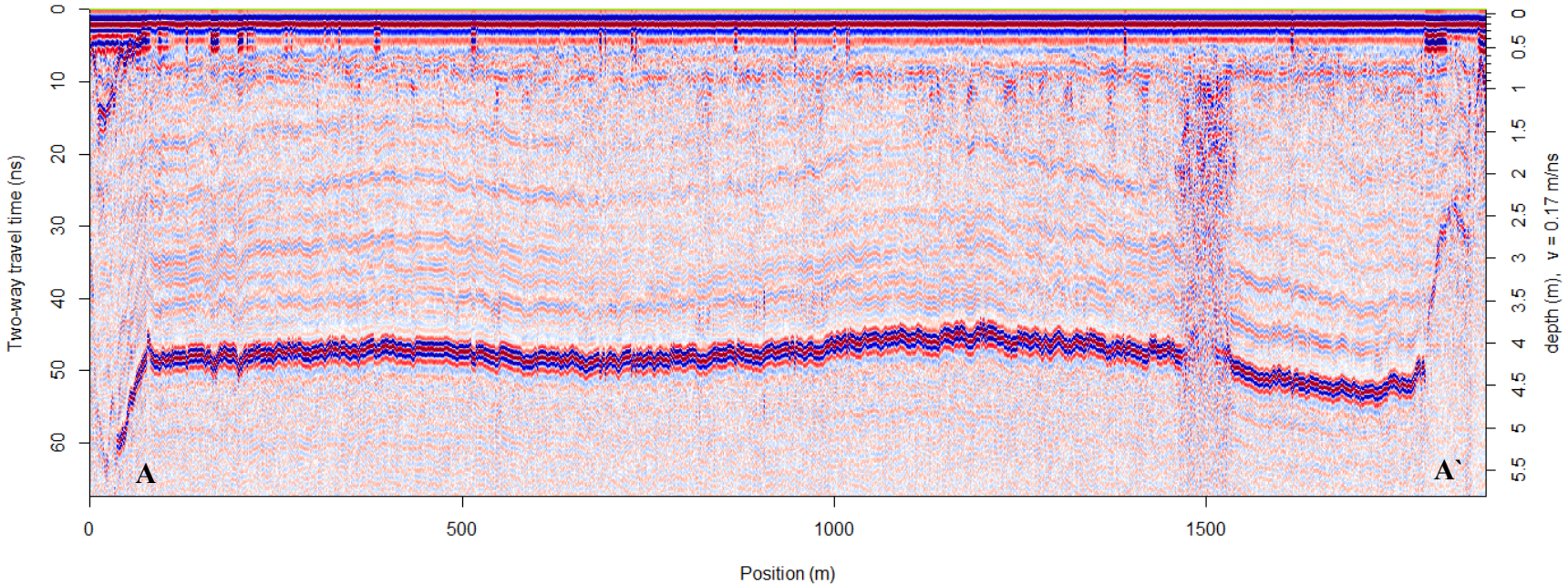

Fig. A3. 6 Ground penetrating radar (GPR) line over Lake Obersee. GPR line acquired over the Lake Obersee ice cover on 10 December 2021 traversing the line from **A** to **A`** in **Fig. 16**. The GPR line shows two relatively thin regions around c. 400 and 1200 m which align with the swirl and annular features in the SAR imagery. GPR system is 500 MHz Sensor and Software shielded by-static transducers. GPR data was processed and visualized using RGPR. Time to depth conversion performed using a propagation velocity of 0.17 m ns^{-1}.

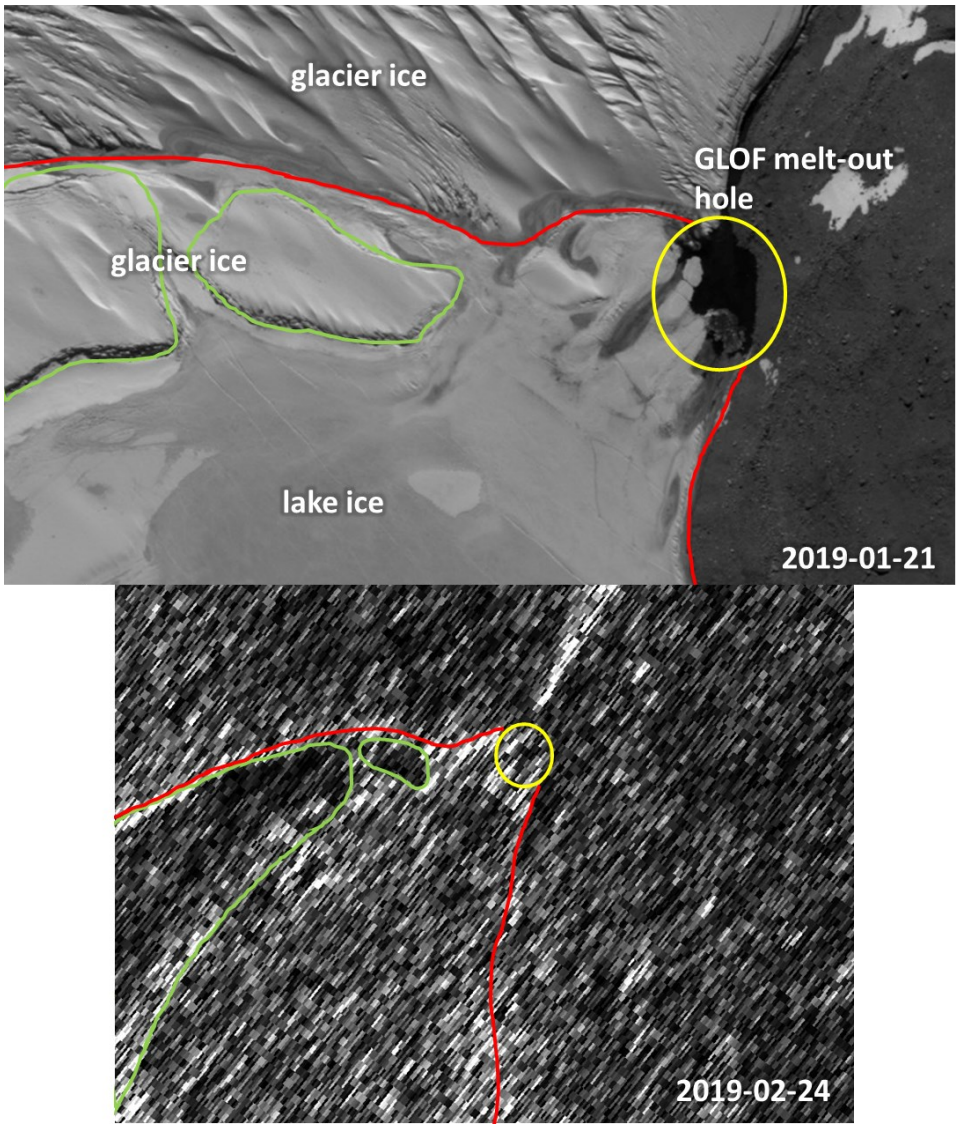

Fig. A3. 7 GLOF melt-out hole at Lake Untersee. The 2018-2019 glacial lake outburst flood (GLOF) that originated from Lake Obersee and drained into Lake Untersee opened a c. 60 × 40 m hole in the north-east corner of the Lake Untersee ice cover. This feature is clearly visible in high resolution optical imagery acquired around the time of the GLOF (**top**). The hole may only be visible in raw Sentinel-1 SLC (slant range geometry) as a small cluster of a few dark resolution cells (**bottom**).

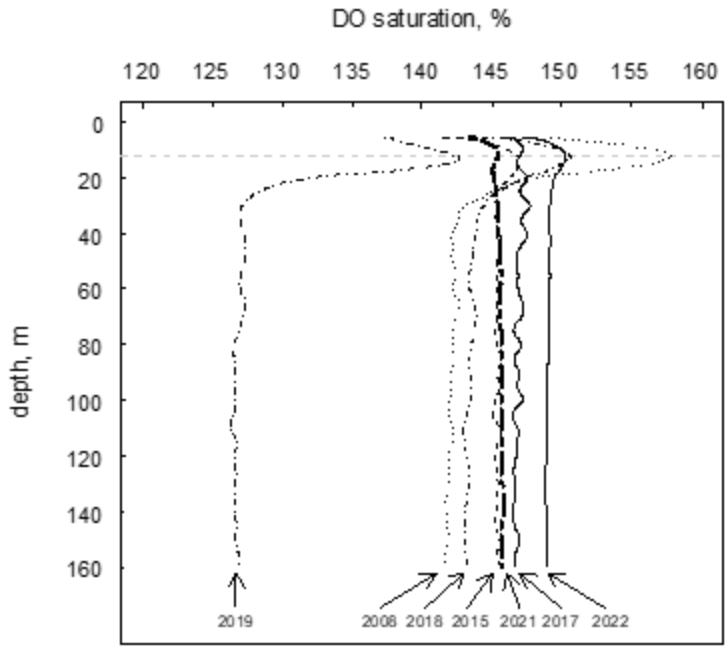

Fig. A3. 8 Dissolved oxygen (DO) profiles of the Lake Untersee water column. Same as **Fig. 8** in the journal manuscript, but additionally includes the profile measured in 2019.